JPL PULSAR TIMING OBSERVATIONS. V. MACRO AND MICROJUMPS IN THE VELA PULSAR 0833−45

J. M. CORDES[1]

Astronomy Department and National Astronomy and Ionosphere Center, Cornell University, Astronomy Department,
University of California at Berkeley, and Astronomy Department, California Institute of Technology

AND

G. S. DOWNS AND J. KRAUSE-POLSTORFF[2]

Jet Propulsion Laboratory, California Institute of Technology

Received 1987 May 12; accepted 1987 December 30

ABSTRACT

JPL pulse timing data extending from 1968 November to 1983 March were analyzed to study the time dependence of the spin frequency. Discontinuities in the spin frequency v have a bimodal amplitude distribution: *macrojumps* (" glitches") occur about once every 1000 days with positive amplitudes $\Delta v/v \approx 10^{-6}$, while *microjumps* of both signs occur 10 times more often with $|\Delta v/v| \approx 10^{-9}$.

We quantify six macrojumps and their associated transients using a 10-parameter model for each jump. Amplitude and decay time parameters vary by a factor ~ 5 over the set of jumps. We find an anticorrelation of -94% between the measured second derivative $\ddot{v}$ and the exponential time constant of one of the transients. We are unable to construct a reliable predictor for macrojumps from the observed parameter values.

Microjumps are identified by demonstrating that they are too large to be mere fluctuations produced by many, much smaller events comprising a random walk process. We suggest that microjumps are, in fact, the basic events that underlie the timing noise of the Vela pulsar. In contrast to macrojumps, which show a signature $(\Delta v, \Delta \dot{v}) = (+, -)$, microjumps show all possible signatures and are not *solely* scaled-down versions of macrojumps.

The results are discussed in terms of superfluid vortex models. Macrojumps are consistent with a model in which angular momentum is suddenly transferred to the crust from a more rapidly rotating superfluid core, followed by relaxation of the rate of spin-down. If the sudden transfers are due to catastrophic vortex unpinning events, then we conclude that the region in which vortices catastrophically unpin must move radially by a few tens of meters in order to produce the observed variations in macrojump parameters. Although vortex events may also underlie microjump activity, some other triggering agent (such as crustquakes) is probably also involved. The constancy of microjump activity in the intervals between macrojumps suggests that the star never reaches quasi-rotational equilibrium.

Subject headings: pulsars — stars: neutron

I. INTRODUCTION

As a rotation driven pulsar, the Vela pulsar is notable for showing pulsed emission throughout the electromagnetic spectrum from radio waves to γ-rays. The pulsar is situated inside the Vela supernova remnant, surrounded by a small synchrotron nebula (Seward 1985). It is among the brightest of radio pulsars in the sky, making it suitable for studies of the radio emission mechanism and magnetospheric structure as well as studies of scattering and Faraday rotation in the interstellar medium. Vela also shows, through the phase of the received pulse train, large discontinuities in its spin rate. In this paper we analyze the rotation of this object in order to further constrain the internal structure of a neutron star.

Soon after its discovery, the Vela pulsar showed an abrupt increase in its spin frequency with an amplitude $\Delta v/v \sim 10^{-6}$ (Reichley and Downs 1969; Radhakrishnan and Manchester 1969). Since this first spin-up (also called a jump or glitch), six others have occurred at a rate of one every few years. These jumps in the rotation frequency ($v \sim 11.2$ Hz) are superposed on the general spin-down rate $\dot{v} \sim -1.6 \times 10^{-11}$ Hz s^{-1} and

are accompanied by jumps in the spin-down rate of $\Delta \dot{v}/\dot{v} \sim 10^{-2}$.

The general behavior of the spin-down is represented in Figure 1 on a coarse scale. Since the last extensive analysis of the first four macrojumps (Downs 1981; henceforth Paper I), three more jumps have been observed (McCulloch *et al.* 1981; Hamilton, McCulloch, and Royle 1982; Klekocink, McCulloch, and Hamilton 1985). The fifth jump has been analyzed in considerable detail (McCulloch *et al.* 1983). One purpose of this paper is to present parameters of the first six jumps as derived from an analysis of arrival time data obtained at the Jet Propulsion Laboratory (Downs and Reichley 1983, hereafter Paper II; Downs and Krause-Polstorff 1986, hereafter Paper IV). We quantify the six macrojumps and discuss the results in terms of the catastrophic vortex unpinning models proposed by Alpar *et al.* (1984*a*, *b*).

In addition to the large (macro) jumps, which have also been seen from six other objects (Boynton *et al.* 1972; Groth 1975; Manchester 1981; Downs 1982; Backus, Taylor, and Damashek 1982; Lyne 1987), many pulsars show lower level "timing noise" (Cordes and Helfand 1980; Cordes and Downs, 1985 hereafter Paper III). Timing noise is similar in behavior to noise in terrestrial oscillators and frequency standards which commonly show frequency fluctuations having power-law
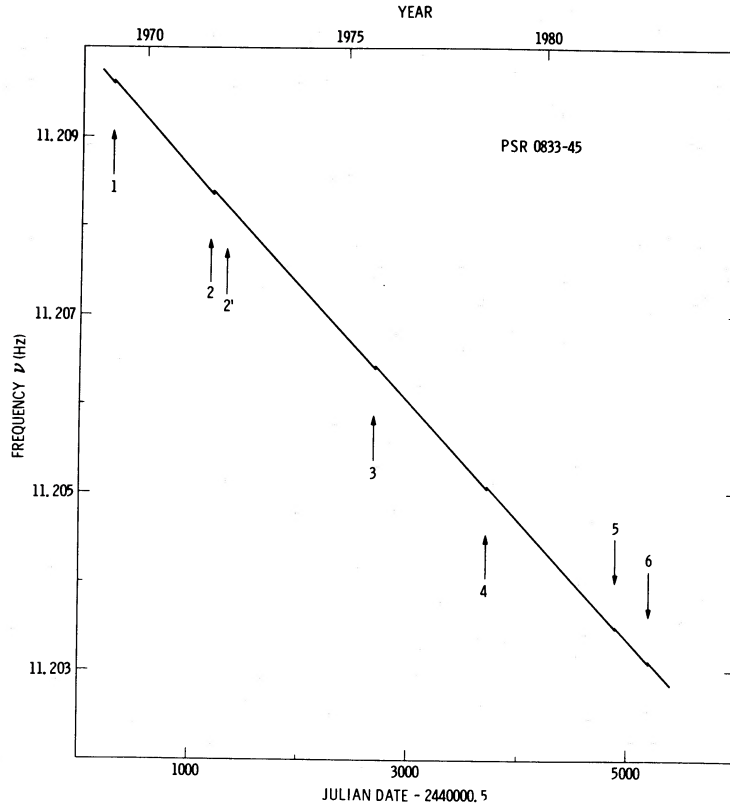

FIG. 1.—General rotation frequency decrease and associated jumps (spin-ups) between 1968 and early 1983, the time encompassed by the JPL timing program. Numbered arrows mark the epochs of *macrojumps* ("glitches").

power spectra (e.g., Rutman 1978). In the case of pulsars, timing noise is roughly consistent with the occurrence of a random walk in either the rotational phase (ϕ), frequency (v), or frequency derivative ($\dot{v}$), or some combination of the three. Paper III analyzed the JPL data of 23 objects (excluding the Vela pulsar) and was able to identify *some* of the timing noise with specific small-amplitude events (which we shall term *microjumps*) in v and $\dot{v}$. Alpar, Nandkumar, and Pines (1986) and Boynton and Deeter (private communication) have also analyzed the JPL timing data, with similar conclusions about microjump behavior. Alpar, Nandkumar, and Pines concluded that microjumps are not simply scaled-down versions of macrojumps.

It is important to develop a complete observational description of microjumps in order to weigh the applicability of models involving neutron star interiors (e.g., Alpar et al. 1984a, b) and torque fluctuations from magnetospheric variability (Cordes and Greenstein 1981; Arons 1981). For this reason, and especially since it is important to understand the relationship of macrojumps and microjumps, we have also analyzed microjumps for the Vela pulsar in considerable detail. The quantification of microjump behavior for this object is much more complicated than for other pulsars because rotational phase deviations from a smooth spin-down model are dominated by macrojumps and their subsequent evolution. Much of the work has involved a careful estimation of the macrojump parameters (which themselves are made uncertain by the microjumps), followed by removal of the macrojumps from the data before study of the microjumps.

In § II we present the analysis of macrojumps, which are generally describable by instantaneous discontinuities in v and

$\dot{v}$ (and sometimes $\ddot{v}$) which exponentially decay with two distinct time constants, superposed on a long-term linear decay. Section III is devoted to an anlysis of timing noise and microjumps. We present a statistical description of timing noise with the use, as in Paper III, of an analysis of variance. We identify and assess the significance of discontinuities in v and $\dot{v}$ and present a list of those that we consider real. In § IV we consider physical modes involving crust quakes and superfluid vortex flows. Section V summarizes the results of the paper.

II. MACROJUMPS

Recently, Alpar et al. (1984b) extracted curves of $\dot{v}$ following each jump from Figure 2 of Paper I and suggested that the decay of $\dot{v}$ consisted of short and intermediate components which meld into a linear decay of $\dot{v}$. Here we carry out a considerably more detailed analysis than that of Paper I, and proceed independently to a similar conclusion. In the following, we present the detailed results on each macrojump and investigate correlations between the 10 parameters that characterize each macrojump and subsequent evolution.

We analyze arrival time data obtained with the Deep Space Network from 1968 to 1983, as described in Downs and Reichley (Paper II) and Downs and Krause-Polstorff (Paper IV). The arrival times were referred to the solar system barycenter through use of the JPL planetary ephemeris DE 96 (Standish, Keesey, and Newhall 1976) and knowledge of the pulsar position. The *optical* position (Manchester et al. 1978) was used because it is more accurate than the radio position. Proper motion was assumed to be zero since no measurements exist to suggest otherwise. The barycentric arrival times appear to be determined by the intrinsic rotational phase of the pulsar and

measurement errors. As we have argued in Paper III, *time variable* contributions from interstellar propagation processes (e.g., Armstrong 1984; Blandford and Narayan 1984; Cordes, Pidwerbetsky, and Lovelace 1986) are negligible for this object. In Paper IV, evidence was found for small (~ 25 μs) fluctuations in phase that were correlated over 1 hour but were uncorrelated from day to day. While the physical interpretation of these perturbations is unknown (and may involve magnetospheric processes), we consider them to be a contribution to the measurement errors in the analysis to be presented.

a) Model for the Spin Frequency

For most nonbinary radio pulsars, barycentric pulse arrival times are analyzed by fitting a simple power series phase model to the arrival times in a least-squares procedure. Expanding in a Taylor series about a reference epoch t_0, the underlying frequency model takes the form

$$v(t) = v_0 + \dot{v}_0(t - t_0) + \ddot{v}_0(t - t_0)^2/2 , \qquad (1)$$

where $\dot{v}_0$ and $\ddot{v}_0$ are the first and second derivatives, respectively, of the frequency at time t_0. Equation (1) is an excellent approximation to the spin-down function expected from electromagnetic braking (Manchester and Taylor 1977) which, for Vela, occurs on a characteristic time $v/|\dot{v}| \sim 23,000$ yr.

The arrival times of the Vela pulsar are significantly affected by perturbations of the simple rotation law. An appropriate model for the spin-down rate, which is justified in the analysis below, can be written as

$$
\begin{aligned}
\dot{v}(t) = \dot{v}_0 &+ \ddot{v}_0(t - t_0) \\
&+ \sum_j \{[\dot{v}_{s_j} e^{-(t - T_j)\tau_{s_j}} + \dot{v}_{i_j} e^{-(t - T_j)/\tau_{i_j}} + \dot{v}_{l_j} \\
&+ \ddot{v}_{l_j}(t - T_j)]U(t - T_j)U(T_{j+1} - t)\} , \qquad (2)
\end{aligned}
$$

where $\dot{v}_0$ and $\ddot{v}_0$ are associated with the general spin-down obtained in the absence of macrojumps and are evaluated at $t = t_0$. In the analysis discussed below, T_j coincides with the first postjump observation since phase continuity is lost after a jump owing to the discrete sampling. The immediate postjump response comprises short and intermediate exponential decays described by the magnitudes $\dot{v}_{s_j}$ and $\dot{v}_{i_j}$. The exponential components decay with time constants τ_{s_j} and τ_{i_j} into the linear component of $\dot{v}$ such that

$$\tau_{s_j} \ll \tau_{i_j} \ll |\dot{v}_{l_j}/\ddot{v}_{l_j}|. \qquad (3)$$

The unit step function $U(t - T_j)$ limits the influence of affected terms to times $t \geq T_j$, while $U(T_{j+1} - t)$ turns off the decay at the epoch T_{j+1} of the next jump.

Thus, each interjump era is treated separately from other eras. The parameters v_{0_j}, $\dot{v}_{0_j}$, and $\ddot{v}_{0_j}$ then refer to the epoch T_j and necessarily change in value at each epoch such that

$$v_{0_j} = v_0 + \dot{v}_0(T_j - t_0) + (\tfrac{1}{2})\ddot{v}_0(T_j - t_0)^2 ,$$

$$\dot{v}_{0_j} = \dot{v}_0 + \ddot{v}_0(T_j - t_0) ,$$

$$\ddot{v}_{0_j} = \ddot{v}_0 .$$

In practice, the separation of the spin-down parameters from those describing the linear portion $\dot{v}_{l_j} + \ddot{v}_{l_j}(t - T_j)$ of the macrojump decay is not possible. We then obtain combined values $\dot{v}_{0_j} + \dot{v}_{l_j}$ and $\ddot{v}_{0_j} + \ddot{v}_{l_j}$ from the fits to the data.

A likely braking index describing the spin-down is $n \equiv v\ddot{v}/\dot{v}^2 \sim 3$ (see Manchester and Taylor 1977), suggesting $\ddot{v}_0 \sim 7 \times 10^{-23}$ Hz s^{-2}, a value that is evidently an order of magni-

tude less than those found for $\ddot{v}_l$. Therefore, while the presence of $\ddot{v}_0$ is acknowledged, we are unable to determine its value because of the transients associated with macrojumps (and microjumps). We argue in § IIe that each linear decay terminates abruptly with the next macrojump.

The spin rate is obtained by integrating equation (2) (while, for notational simplicity, we drop the sum over all jumps), obtaining $v(t) = \int dt \, \dot{v}(t) + \text{constant}$, where the constant of integration is such that $v(t = T_j) = v_{0_j}$. The phase of the pulsar signal is obtained by another integration, yielding

$$
\begin{aligned}
\phi(t) = &\int v(t) + \text{constant} \\
= &\, \phi_{0_j} + v_{0_j}t + (\dot{v}_{0_j} + \dot{v}_{l_j})t^2/2 + (\ddot{v}_{0_j} + \ddot{v}_{l_j})t^3/6 \\
&+ \dot{v}_{s_j}\tau_{s_j}[t + \tau_{s_j}(e^{-t/\tau_{s_j}} - 1)] + \dot{v}_{i_j}\tau_{i_j}[t + \tau_{i_j}(e^{-t/\tau_{i_j}} - 1)] ,
\end{aligned}
$$
$$(4)$$

where t is now measured relative to T_j as discussed above, and where the constant of integration is chosen such that $\phi(t = T_j) = \phi_{0_j}$. For simplicity in the discussion below, we drop the subscript j and the parameters are understood to apply only to a particular postjump interval.

Jump 2′ is apparently linearly superposed on the decay following jump 2 (see § IId). Therefore, jumps 2 and 2′ are modeled together as in equation (2) except that only the short-term decay following jump 2′ is retained. We then obtain a spin-up due to jump 2′

$$v_p(t) = \{\Delta v_p - \dot{v}_{sp}\tau_{sp}[e^{-(t - T_p)/\tau_{sp}} - 1]\}U(t - T_p) , \qquad (5)$$

where Δv_p is the measured spin-up at epoch T_p, $\dot{v}_{sp}$ refers to epoch $t = T_p$, and the subscript p refers to jump 2′. The contribution ϕ_p to the phase is then

$$
\begin{aligned}
\phi_p(t) = \phi_{0_p} + \{(\Delta v_p + \dot{v}_{sp}\tau_{sp})(t - T_p) \\
+ \dot{v}_{sp}\tau_{sp}^2[e^{-(t - T_p)/\tau_{sp}} - 1]\}U(t - T_p) , \qquad (6)
\end{aligned}
$$

where ϕ_{0_p} (the phase at $t = T_p$) takes into account the fact that we do not know the actual jump epoch or the history of the decay up until the first postjump observation.

b) Jump Parameters

It would be easy to recognize a macrojump during observations because, for an amplitude $\Delta v/v \sim 10^{-6}$, the observed phase drifts by one pulse width (~ 3.3 ms) after $\sim 37,000$ periods (~ 1 hr for Vela). Unfortunately, none of the macrojumps occurred during an observing session, and more than one cycle of phase was lost between observing sessions that bracket any of the macrojumps. Therefore, macrojumps were identified in the JPL data by making fits of equation (1) to subsets of the available samples and finding the epoch at which the fits became catastrophically poor.

Subsequently, two model fits were made, the first to the data spanning 30 to 90 days just prior to the jump, and the second to the first four observation days following the jump. In all cases the rms residual after each model fit was 20–25 μs. Model parameter differences (Δv, $\Delta \dot{v}$, and $\Delta \ddot{v}$) across each jump, listed in Table 1, were computed by extrapolating the prejump model parameters to the earliest postjump epoch (col. [3]) and subtracting from the postjump parameters. The estimated errors in Table 1 are due primarily to random phase variations inherent in the pulse train (see Paper IV), *not* due to noise extrinsic to the pulsar.

TABLE 1

LARGE JUMP PARAMETERS FOR PSR 0833−45[a]

	JUMP EPOCH[b] (JED—2,440,000)		ROTATIONAL PARAMETERS			PERIOD PARAMETERS		
JUMP	After	Before	$\Delta\nu$ $(10^{-7}$ Hz$)$	$\Delta\dot\nu$ $(10^{-13}$ Hz s$^{-1})$	$\Delta\ddot\nu$ $(10^{-22}$ Hz s$^{-2})$	ΔP $(10^{-9}$ s$)$	$\Delta\dot P$ $(10^{-15}$ s s$^{-1})$	$\Delta\ddot P$ $(10^{-24}$ s s$^{-2})$
1.........	276.75	283.69	261.81(0.96) ± 0.03	−1.58(−0.20) ± 0.05	347 ± 54	−208.35(−0.77) ± 0.02	1.25(0.16) ± 0.04	−276 ± 43
2.........	1185.27	1199.23	229.18(3.37) ± 0.01	−2.32(−0.94) ± 0.03	782 ± 19	−182.43(−2.68) ± 0.01	1.84(0.75) ± 0.02	−622 ± 15
2′........	1308.94	1315.87	1.34(0.21) ± 0.01	−0.30(−0.09) ± 0.03	143 ± 20	−1.06(−0.16) ± 0.01	0.31(0.07) ± 0.02	−114 ± 16
3.........	2680.50	2685.67	222.48(0.84) ± 0.04	−1.66(−0.11) ± 0.09	214 ± 76	−177.16(−0.67) ± 0.03	1.32(0.08) ± 0.07	−170 ± 61
4.........	3681.40	3704.32	342.90(7.13) ± 0.01	−2.87(−1.46) ± 0.03	736 ± 24	−273.12(−5.67) ± 0.01	2.28(1.16) ± 0.02	−586 ± 19
5.........	4888.49	4889.30	127.44(0.09) ± 0.01	−1.32(−0.01) ± 0.01	169 ± 11	−101.53(−0.07) ± 0.01	1.05(0.01) + 0.01	−134 ± 9
6.........	5191.58	5192.56	229.61(0.31) ± 0.01	−3.61(−0.16) ± 0.04	1897 ± 45	−182.94(−0.25) ± 0.01	2.87(0.13) ± 0.03	−1511 ± 36

[a] 2 σ errors.

[b] From epochs published by Downs 1981, Manchester, Goss and Hamilton 1976, Hamilton, McCulloch, and Royle 1982, McCulloch et al. 1983, and McCulloch 1986.

Values for the period parameter changes (ΔP, etc.) across a jump are included in Table 1 for comparison with the earlier values tabulated in Paper I. (Conversions between $\Delta\nu$ and ΔP and their time derivatives are discussed in Appendix A.) Slight differences are due mainly to the decision to confine the post-jump fit to only the first four observation days following a jump. Another contribution comes from use of the optical position of the pulsar rather than the radio position used in Paper I.

Uncertainty in the jump epoch causes an additional uncertainty in the jump parameters. To estimate these possible parameter corrections, the postjump model parameters were backdated to the earliest epoch the jump could have occurred (col. [2] in Table 1), while the prejump parameters were updated to the same epoch and again subtracted. The differences between the listed changes and these later estimates appear in parentheses in Table 1. The systematic errors can in fact be much larger. McCulloch et al. (1983) have analyzed a set of daily observations (the JPL observations were weekly) around jump 5, thereby detecting a small but significant exponential component of the jump which exhibits a decay time of

1.6 day. The total $\Delta\nu$ reported by them exceeds that reported here by the amount of the fast-decaying component. The JPL observations missed the jump by 0.8–1.5 day. According to preliminary results of Hamilton, McCulloch, and Royle (1982), the JPL observations missed jump 6 by 1.1 day, so a strong short-term component may also contribute to jump 6.

c) Postmacrojump Evolution of $\dot\nu$

Figures 2–6 trace the rapid changes in $\dot\nu$ immediately following the six macrojumps. The plotted values were obtained by fitting second-order phase models to three successive days of observation with the origin of each fit moved to later times at ~1 week intervals (the typical interval between observations). About 150–200 days after a jump the initial transient has diminished, so third-order fits over extended intervals (30–90 days) are possible. The results of these fits, wherein the rms residual was again typically 25 μs, are represented by the connected symbols in Figures 2–6.

In each figure a single data point is plotted 5 days before each jump and represents the value of $\dot\nu$ predicted by the prejump behavior at the jump epoch. The value is based on a
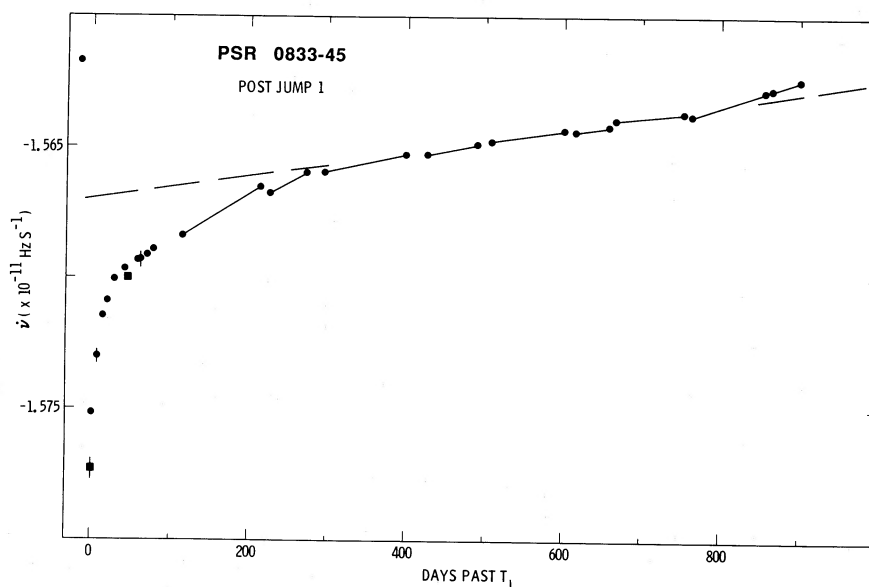

FIG. 2.—Spin-down rate $\dot\nu$ following macrojump 1 and preceeding macrojump 2. Filled circles: Second-order fits. Connected filled circles: third-order fits over long spans. Filled squares: Third-order fits over restricted spans. Error bars are shown where large enough and are ±2 σ. Broken line: estimate of linear behavior.
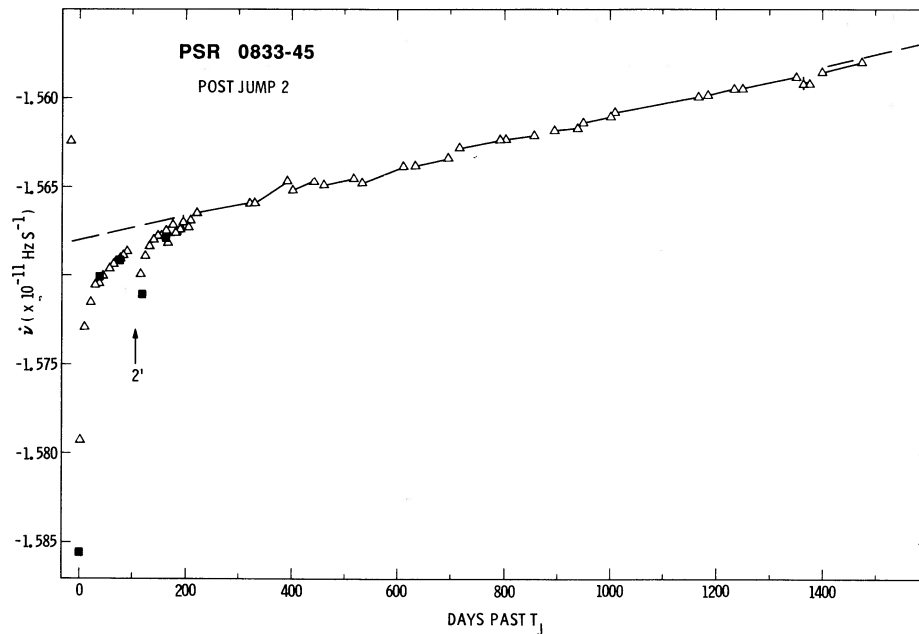
FIG. 3.—Spin-down rate $\dot{\nu}$ following macrojump 2 and preceeding macrojump 3. *Open triangles:* second order fits. *Connected open triangles:* third order fits over long spans. *Filled squares:* third order fits over restricted spans. Error bars are shown where large enough and are $\pm 2\,\sigma$. *Broken line:* estimate of linear behavior.

third-order model fit to the 30–60 days prior to the jump. A comparison of this value to one obtained from a third-order fit using the first four observation days following each jump (shown as a filled square) yields the jump in $\dot{\nu}$ presented in Table 1. Occasionally, other third-order fits using four successive observation days were made as a check on the stability of the results of the second-order fits. These results are also plotted as filled squares in Figures 2–6.

d) Postjump Parameters

Short and intermediate-term decays of $\dot{\nu}$ are evident in Figures 2–6: a short-term decay of a few days is followed by a longer, intermediate-term decay of 100 to 200 days. To investigate this behavior quantitatively we present the long-term linear decay as $\dot{\nu}_{\mathrm{lin}}(t) = \dot{\nu}_l + \ddot{\nu}_l t$. We then computed the difference $\dot{\nu}_d(t) = \dot{\nu}(t) - \dot{\nu}_{\mathrm{lin}}(t)$ to decouple the long-term decay from
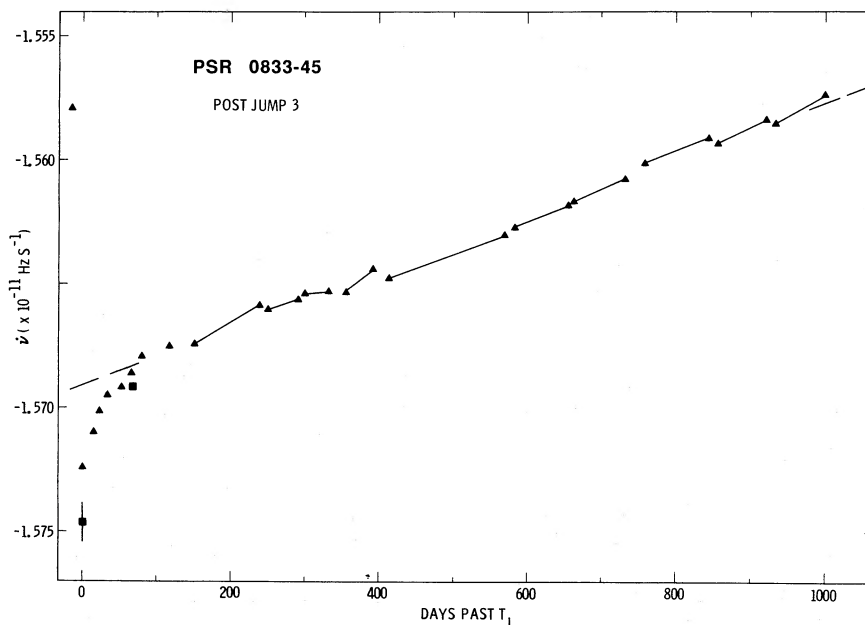

FIG. 4.—Spin-down rate $\dot{\nu}$ following macrojump 3 and preceeding macrojump 4. *Filled triangles:* second-order fits. *Connected filled triangles:* Third-order fits over long spans. *Filled squares:* third-order fits over restricted spans. Error bars are shown where large enough and are $\pm 2\,\sigma$. *Broken line:* estimate of linear behavior.
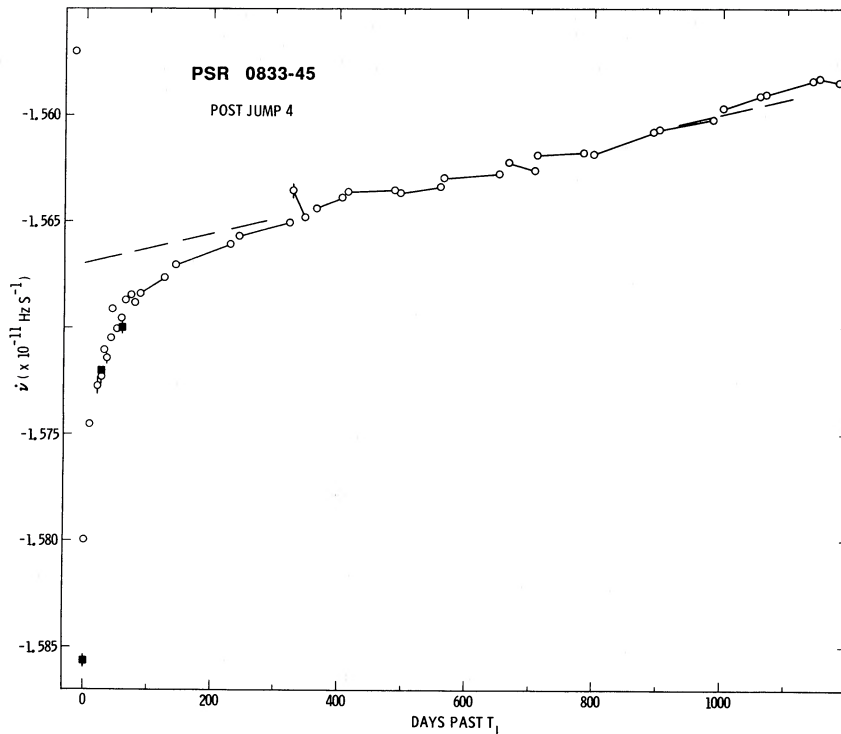
FIG. 5.—Spin-down rate $\dot{\nu}$ following macrojump 4 and preceeding macrojump 5. *Open circles:* second-order fits. *Connected filled circles:* third-order fits over long spans. *Filled squares:* third order fits over restricted spans. Error bars are shown where large enough and are $\pm 2\,\sigma$. *Broken line:* estimate of linear behavior.

the earlier transient decay. The magnitude $|\dot{\nu}_d|$ is displayed in Figures 7–10 on semilog scales, wherein an *intermediate-term exponential decay* of $\dot{\nu}$ is clearly visible as a linear trend following each jump. A clear and separate *short-term decay* is also present therein, but the data are insufficient following all jumps to test the exponential form for the short-term decay. Nevertheless, the short-term decay is modeled as such since McCulloch *et al.* (1983) have modeled the postjump 5 decay with, in part, a short-term (~ 1 day) exponential with some success. In Figure 8, and to some extent in Figure 3, we see the basis for treating jump 2' in § IIa as superposed on the decay following jump 2. This jump clearly decays rapidly into a linear extrapolation (on the semilog plot) of the intermediate-term decay of jump 2.

Attempts have also been made to fit an exponential decay model to the *long*-term (200–1400 days) behavior of the Vela pulsar (Manchester 1981, and most recently, McCulloch *et al.* 1983). The case was made in Paper I, however, that the magnitude of $\dot{\nu}$ (as opposed to ν) decreases *linearly*, not exponentially, with time for hundreds of days prior to the next jump. The dynamics following each jump have been displayed in terms of the spin-down rate $\dot{\nu}$ after each jump in Figures 2–6 to make this point clear. Dashed lines therein represent fits to the linear decay (tentative in the case of postjump 6 due to a lack of data). There is *no* evidence for a *long-term exponential* decay in the data; if the long-term decay is in fact exponential, then the time constant must be at least 50 yr. Fluctuations in $\dot{\nu}$ away from linearity appear to be due entirely to microjump fluctuations.

The results of the model fitting of equation (4) are presented in Table 2 and Figures 7–10. The table gives values of the jump parameters and the rms phase residual following removal of the model from the data. As discussed below, the phase

residuals are more than two orders of magnitude larger than typical measurement errors and are dominated by microjumps.

In Figures 7–10, the models are shown as solid lines, representing the intermediate-term decays, and are limited in time to indicate the data points used in selecting the parameter values. Short-term decays are represented as dashed curves, while jump 2' is the solid curve in Figure 8. Formal statistical errors were possible only for the indicated parameters in Table 2. In these cases nonlinear least-squares fitting was performed. The remaining parameters were evaluated as described below, and in these cases the error was evaluated by experimentation. We emphasize that the short-term decays are poorly sampled, so the listed parameter values are most certainly subject to unknown systematic errors.

The fitting procedure was complicated by the timing noise due to microjumps. Preliminary evidence of this noise appears in Figures 2–6, where measurement error is several orders of magnitude below the observed fluctuations. In the sense that timing noise is not modeled, the phase model is incomplete, so it is not possible to obtain parameter values which are free of significant perturbation. In some cases the least-squares results were heavily dependent on the assumed initial values. For example, following jump 1, least-squares solutions for ϕ_0 and τ_i simultaneously yielded values for τ_i of 124.3 ± 3.6, 115.4 ± 1.6, 98.8 ± 0.8, and 91.1 ± 1.7 days for initial values of 105, 110, 120, and 125, days, respectively. Furthermore, the amount of data available for the short-term decays is so sparse that attempts to solve for $\dot{\nu}_s$ and τ_s resulted in unstable computations. Thus, while the long-term decay parameters ν_0, $\dot{\nu}_0 + \dot{\nu}_l$, and $\ddot{\nu}_0 + \ddot{\nu}_l$ were determined in a conventional iterative least-squares procedure, the exponential parameters $\dot{\nu}_s$, τ_s, $\dot{\nu}_i$, and τ_i were selected in a hybrid (manual and least-squares) process.
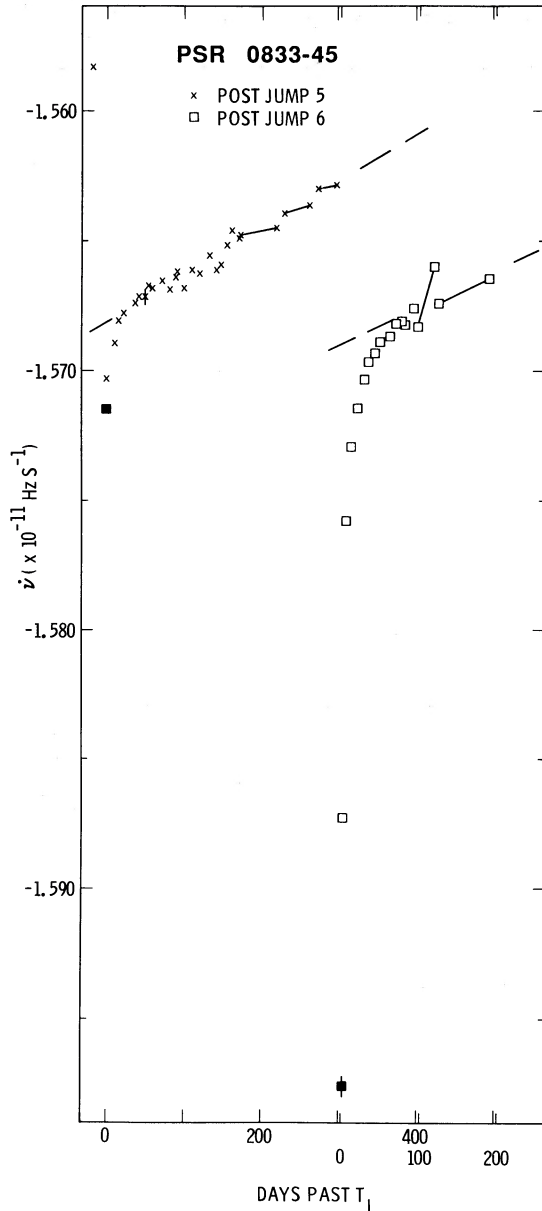
FIG. 6.—Spin-down rate $\dot{v}$ following macrojumps 5 and 6. *Crosses:* jump 5. *Open squares:* jump 6. *Unconnected points:* second-order fits. *Connected points:* third-order fits over long spans. *Filled squares:* third-order fits over restricted spans. *Broken lines:* estimates of linear behavior. Error bars are shown where large enough and are $\pm 2\sigma$.

One iteration of this procedure consisted of (1) fit v_0, $\dot{v}_0 + \dot{v}_l$, $\ddot{v}_0 + \ddot{v}_l$ and ϕ_0 by least squares, using prior estimates of $\dot{v}_s$, τ_s, $\dot{v}_i$, and τ_i (on the first pass the values of $\dot{v}_0 + \dot{v}_l$ and $\ddot{v}_0 + \ddot{v}_l$ were selected by inspection of data in Figs. 2–6, while the exponential parameters were evaluated using earlier versions of Figs. 7–10.); (2) evaluate $|\dot{v}_d|$; (3) determine $\dot{v}_i$ and a first guess of τ_i by a linear least-squares fit to log ($|\dot{v}_d|$) in the range of applicability (see Figs 7–10); (4) adjust τ_i using plots of δv versus time as an aid in selecting the "minimum perturbation" (see Appendix B for more discussion on this point); (5) obtain $\dot{v}_s$ from the fact that $\dot{v}_d(0) = \dot{v}_s + \dot{v}_i$; (6) select τ_s from a visual linear fit to the appropriate data in Figures 7–10. This procedure was performed for two iterations to arrive at values in Table 2.

e) Correlations between Macrojump Parameters

Alpar *et al.* (1981) presented a strong linear correlation (0.95) between the observed time interval t_g between macrojumps and that predicted from the observed $\Delta\dot{v}$ (labeled t_g^{th} therein). This led to a *predicted* jump 5 epoch of between 1985 February and 1985 August whereas the *observed* jump epoch was about 12 October 1981 (3.5 years earlier). However, their prediction was based on jump parameter values which differ (in one case substantially) from those in Table 1. Using our values in their analysis we would have predicted a jump epoch near 1982 November, somewhat closer to the observed epoch. In any case, we find the correlation between t_g and t_g^{th} for six macrojumps to be downgraded to 0.55.

We consider observations *during* a macrojump to be of high importance, but a method of predicting the jump epoch is required in light of limited observing resources. We investigated several other parameter correlations in the hope that a predictor for the macrojump epoch could be constructed. The coefficient ρ describing the correlation of parameters p and q is written below as $\rho(p, q)$. Few significant correlations were found. The computed correlations are listed in the correlation matrix of Table 3. All parameters except v_l and v_d have been defined earlier. Here $v_l = \ddot{v}_l t_g^2/2$ is the total change in rotation frequency associated with the linear decay, which may be due to a process different from those associated with the exponential decays. (At this point we ignore any contribution to $\ddot{v}$ from the external magnetospheric torque, which is likely to be 10 times smaller than $\ddot{v}_l$, as argued above). The parameter $v_d \equiv \int dt\, \dot{v}_d$ is discussed below. Most of the correlations are between parameters pertaining to a particular jump and its postjump era. In some cases, correlations between parameters of different jumps are made. We designate these with a plus or minus, where a minus denotes values of the quantity in a column chosen from the *preceding* jump, while a plus implies values taken from the following jump. As is clear, few of the correlations appear statistically significant. The exceptions are now discussed, one relating to data consistency and one relating to the internal dynamics of the star.

Given a purely exponential response, one would expect transient derivatives ($\dot{v}_s$, $\dot{v}_i$) to be directly related to the presumed stimulus (Δv). We found $\rho(\Delta v, \dot{v}_i) \approx 0.95$ for jumps 1–5. Adding jump 6, $\rho \approx 0.68$. Inspection of Figure 10 suggests that $\dot{v}_i$ may be biased high at the expense of τ_s, which may be biased low. Letting $\dot{v}_i \approx -5 \times 10^{-14}$, then $\rho \approx 0.88$, a reasonably high correlation. We find $\rho(\Delta v, \dot{v}_s)$ low, but $\dot{v}_s$ is poorly determined due to sparse sampling, so this result is not surprising.

Of some surprise, however, is a strong correlation between the linear decay and the time constant of the intermediate exponential decay: $\rho(\ddot{v}_l, \tau_i) \approx -0.94$, using the values of Table 2. The relationship between these parameters is of the form $\ddot{v}_l = K\tau^\alpha$ over the range of available values. Fitting a line by least squares to the logarithm of the values (shown as closed circles in Fig. 11), we obtain $K = 100^{+50}_{-35} \times 10^{-22}$ and $\alpha = -0.6 \pm 0.1$ (quoted errors are 95% confidence limits). That is, a rapid decay results in a larger linear variation in torque, and vice versa. To alleviate concern that the correlation between $\ddot{v}_l$ and τ_i is caused by their simultaneous presence in the phase model, we independently computed the values of $\ddot{v}_l$ by averaging the values obtained in the postjump regions for which third-order fits were obtained (the connected segments in Figs 2–6). We used only segments beginning at times $t > t_c$, where t_c is the time at which the contribution to $\ddot{v}$ due to the intermediate-term decay is only $0.1\ddot{v}_l$. The total effect of the

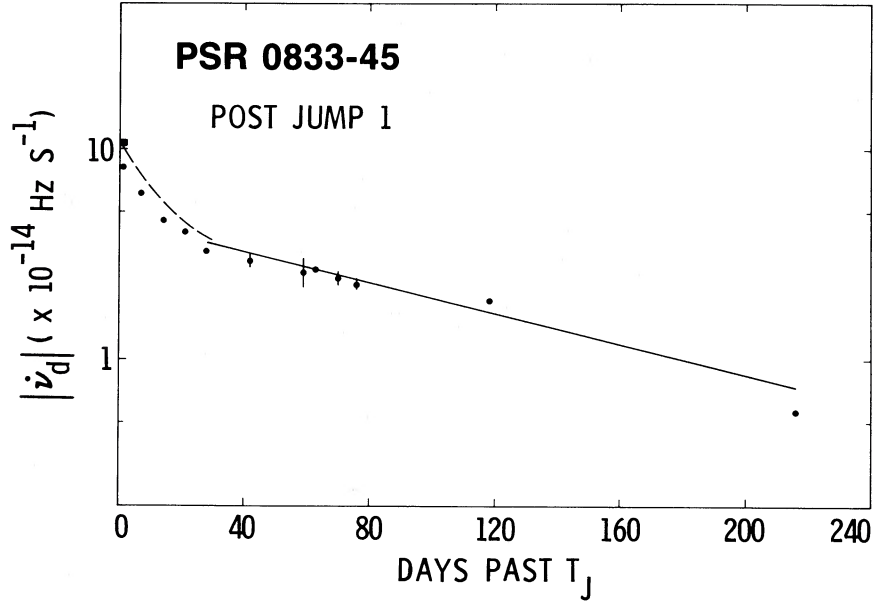FIG. 7.—Semilog plot of the magnitude of the differential spindown rate $\dot{v}_d$ following jump 1. *Filled circles:* second- and third-order fits. *Filled squares:* third-order fit over first four observation days. *Broken line:* model of short term decay. *Solid line:* model of intermediate term decay. Error bars are $\pm 2\,\sigma$.

tails of this decay in biasing values of $\ddot{v}_l$ is then much less than 10%. Following jump 5 several events in $\dot{v}$ contribute to the effective value of $\ddot{v}$, so we made a third-order fit to the last 150 days of that interval. Using these values of $\ddot{v}_l$, we find $\rho(\ddot{v}_l, \tau_i) = -0.89$, thus confirming the original result. These data points are also shown in Figure 11 (*open circles*) with error estimates which primarily take timing noise into account. The extreme values allow correlation values between $-0.92 < \rho < -0.84$.

We then asked whether the total decay (short plus intermediate) is related to $\ddot{v}_l$. We therefore computed numeri-

cally $v_d = \int dt\, \dot{v}_d$ (i.e., the integrals of the curves in Figs 7–10). We obtain, for jumps 1–6 $v_d \times 10^7 = (-4.3 \pm 0.4)$ Hz, (-3.6 ± 0.5) Hz, (-0.7 ± 0.1) Hz, (-5.4 ± 0.3) Hz, (-0.2 ± 0.1) Hz and (-1.65 ± 0.1) Hz, respectively. Thus, $\rho(\ddot{v}_l, v_d) \approx -0.87$, still a significant correlation.

The strongest implication of the large value of $\rho(\ddot{v}_l, v_d)$ is that $\ddot{v}_l$ measured in a particular postjump era, pertains *only to that era*. That is, at the time of the macrojump, all memory of the prejump value of $\ddot{v}_l$ is lost. (Correlating $\ddot{v}_l$ with prior and next-jump values of τ_i, we obtain $\rho = -0.2$ and -0.38, respectively). In the context of the model of Alpar *et al.* (1984a,
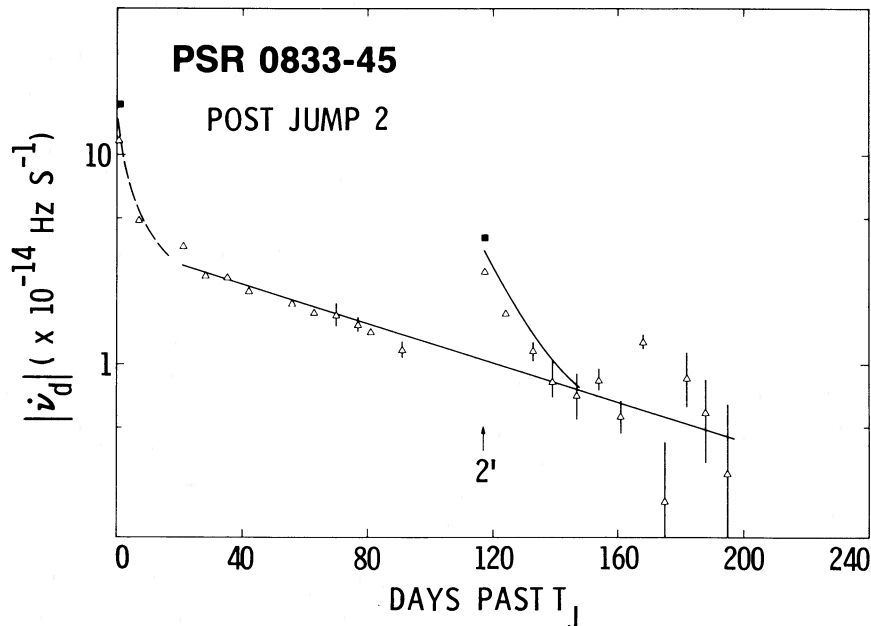

FIG. 8.—Semilog plot of the magnitude of the differential spin-down rate $\dot{v}_d$ following jumps 2 and 2'. *Open triangles:* Second- and third-order fits. *Filled squares:* third-order fit over first four observation days following jumps 2 and 2'. *Broken line:* model of short-term decay following jump 2. *Solid line:* model of intermediate term decay. *Solid curve:* model of short-term decay following jump 2'. Error bars are $\pm 2\,\sigma$.
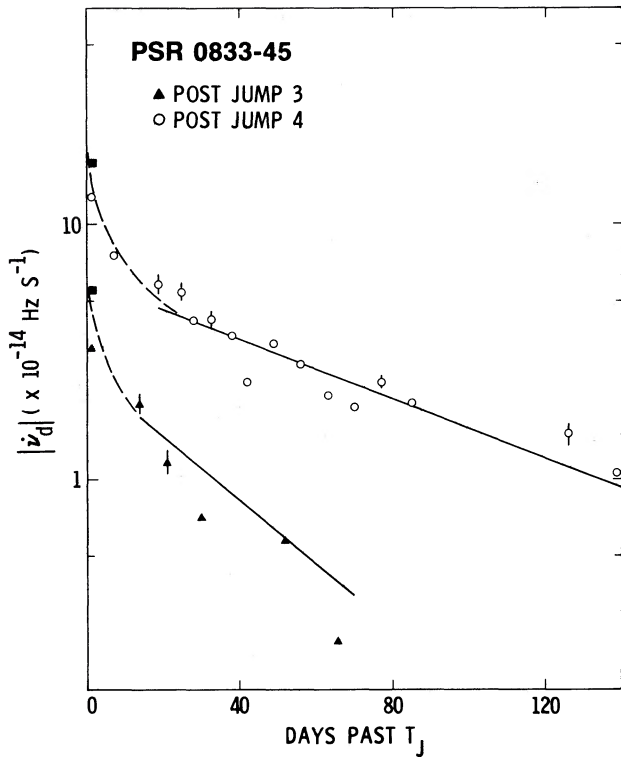
FIG. 9.—Semilog plot of the magnitude of the differential spin-down rate $\dot{\nu}_d$ following jumps 3 and 4. *Filled triangles:* jump 3—second- and third-order fits. *Open circles:* jump 4—second- and third-order fits. *Filled squares:* third-order fit over first four observation days. *Broken lines:* models of short-term decays. *Solid lines:* model of intermediate-term decays. Error bars are $\pm 2\sigma$.
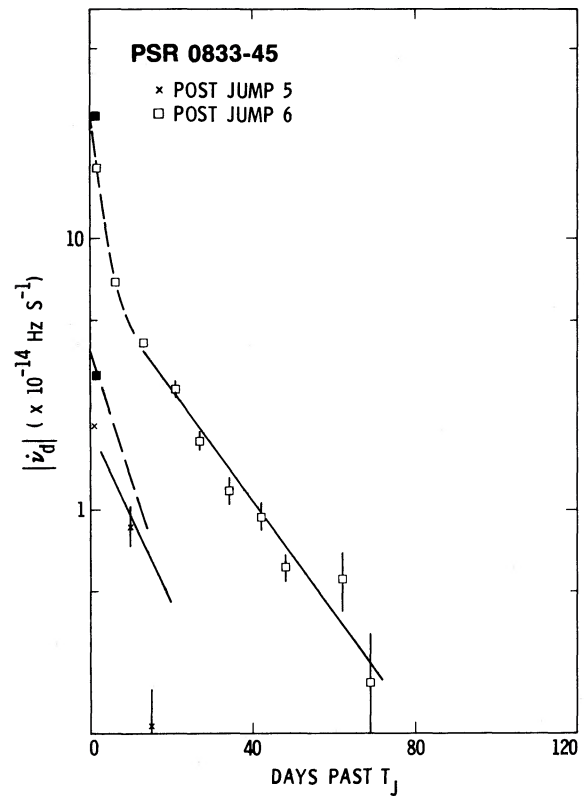

FIG. 10.—Semilog plot of the magnitude of the differential spin-down rate $\dot{\nu}_d$ following jumps 5 and 6. *Crosses:* jump 5—second- and third-order fits. *Open squares:* jump 6—second- and third order fits. *Filled squares:* third-order fit over first four observation days. *Broken lines:* model of short-term decay. *Solid line:* model of intermediate-term decay. Error bars are $\pm 2\sigma$.

TABLE 2

PARAMETER VALUES FOR ROTATION MODEL OF PSR 0833−45

POST JUMP	LONG-TERM DECAY[a]			EXPONENTIAL DECAY[b]				rms RESIDUAL $(10^{-3}$ cycles$)$
	ν_0 (Hz)	$\dot{\nu}_0 + \dot{\nu}_l$ $(10^{-11}$ Hz s$^{-1})$	$\ddot{\nu}_0 + \ddot{\nu}_l$ $(10^{-22}$ Hz s$^{-2})$	$\dot{\nu}_s$ $(10^{-14}$ Hz s$^{-1})$	τ_s (days)	$\dot{\nu}_i$ $(10^{-14}$ Hz s$^{-1})$	τ_i (days)	
1........	11.20962150449 ±88	−1.5670026 ±54	5.301 ±14	−6.00 ±0.55	10.0 ±1.0	−4.50 ±0.25	120.0 ±6.0	143.1
2........	11.20840613715 ±140	−1.5680110 ±51	8.602 ±8	−10.50 ±0.60	4.0 ±1.0	−3.70 ±0.50	94.0 ±5.0	212.7
2′........	0.00000013100 ±500	0.0000000	0.000	−2.50 ±0.30	10.0 ±0.5	0.00	0.0	212.7
3........	11.20642053333 ±686	−1.5691413 ±358	13.193 ±80	−2.80 ±0.30	4.0 ±0.4	−2.60 ±0.20	35.0 ±2.0	132.1
4........	11.20507908692 ±182	−1.5669843 ±77	8.037 ±14	−16.00 ±1.60	6.0 ±0.6	−6.00 ±0.30	75.0 ±3.0	96.2
5........	11.20349067793 ±97	−1.5682267 ±171	21.060 ±130	−2.00 ±0.20	6.0 ±0.6	−2.00 ±0.30	14.0 ±2.0	7.1
6........	11.20310323706 ±226	−1.5689134 ±680	16.047 ±836	−22.00 ±0.30	3.0 ±0.6	−6.80 ±1.00	21.5 ±2.0	44.0

[a] Errors are $\pm 2\sigma$.
[b] Errors are determined by inspection.

TABLE 3

Cross Correlation Coefficients of Model Parameters[a]

	$\Delta\nu$	$\Delta\dot\nu$	$\dot\nu_i$	τ_i	t_g	$\ddot\nu_l$	ν_d	ν_l
$\Delta\nu$	1.00	0.49	0.95	0.57	0.67	0.30(−)	0.86	0.40
$\Delta\dot\nu$	...	1.00	0.89	−0.12	0.55(−)	−0.08	0.25	−0.64
$\dot\nu_i$	...	...	1.00	0.17	0.57	−0.34	0.55	−0.23
τ_i	...	...	...	1.00	0.62	−0.94	0.83	0.23
t_g	...	...	...	...	1.00	−0.70	−0.65	...
$\ddot\nu_l$	...	...	...	−0.20(−) −0.30(+)	...	1.00	−0.87	...
ν_d	...	...	...	...	0.23(−)	...	1.00	−0.27
ν_l	0.53(+)	...	...	...	...	...	0.15(−)	1.00

[a] See text for definitions of the parameters and of the (−) and (+) symbols.

b), this result also suggests a dynamical connection between the region(s) determining the short and intermediate decays and that region determining the linear decay such that if the spin-up is not suitably relaxed by the earlier decays, the later linear decay responds accordingly. Clearly, this result needs to be confirmed using data collected elsewhere, since at least one more macrojump has occurred since the JPL observations terminated in 1983 March (Klekocink, McCulloch, and Hamilton 1985).

In Paper I a significant correlation between $\ddot\nu_l$ and $\Delta\nu$ of the next jump was found using data from jumps 1–4. With the addition of two more jumps we find $\rho(\ddot\nu_l, \Delta\nu) \approx 0.3$, so that observed correlation is weak. This negative result is based on the assumption that the observed values of $\Delta\nu$ are free from bias due to an unobserved fastly decaying component. We *know*, however, that estimates for $\Delta\dot\nu$ from the JPL data are probably biased due to the postjump decay that occurs faster than the 1 week sample time.

We find no significant correlation of t_g with any single parameter. In computing the correlations we use the fact that

jump 7 occurred within 1 day of MJD 6257 (Klekocink, McCulloch, and Hamilton 1985). It may well be that a particular combination of parameters will correlate strongly with t_g. We attempt such a combination here with no success. Immediately preceeding jumps 1–6 the value of $\dot\nu$ lies entirely within the range $(1.560 \pm 0.003) \times 10^{-11}$ Hz s^{-1}. This suggests a critical value $\dot\nu_{cr}$ must be reached by $\dot\nu_{lin}$ before a macrojump can occur. If this were a firm rule, then the jump will occur at $\hat t_g = (\dot\nu_{cr} - \dot\nu_l)/\ddot\nu_l$. One then hopes for a high value of $\rho(\hat t_g, t_g)$. In fact, using the data from Table 2 for jumps 1–5, we find $\rho(\hat t_g, t_g) = 0.78$, the maximum obtainable with these data, requiring $\dot\nu_{cr} = -1.56250 \times 10^{-11}$ Hz s^{-1}. The rms value of $\hat t_g - t_g$ is 350 days. (Data on jump 6 are omitted here since the observed time span following that jump is short.) The moderate correlation and high rms deviation appears to be caused by the shallow decay in $\dot\nu_{lin}$ in the presence of timing noise: therefore, a small change in $\dot\nu$ translates into a large change in time. Furthermore, $\dot\nu_{cr}$ may not be a constant. Nevertheless, we note that this hypothesis does offer an explanation as to why jump 6 occurred so soon after jump 5: the large value of $\ddot\nu_l$ caused $\dot\nu$ to cross the threshold after a much shorter time than for other macrojumps.

III. TIMING NOISE AND MICROJUMPS

The models of postjump decay presented in § II do not completely model the rotational behavior of PSR 0833−45. We studied additional fluctuations in the spin frequency v and its derivative $\dot\nu$ by numerically differentiating phase residuals $\delta\phi(t)$ after removal of the spin-down and macrojump model of § II. The resultant derivatives—designated $\delta v(t)$ and $\delta\dot\nu(t)$—are shown in Figures 12–17. Differentiation was accomplished by using coefficients of short polynomial fits performed over time spans of 10–60 days (depending on the sampling of the phase). The horizontal error bars in Figures 12–17 represent the lengths of such fits, and the vertical error bars are $\pm 1 \sigma$ errors, where σ is the formal error. In order to enhance the short-term fluctuations (which are the subject of this section), we have detrended the δv curves by removing a running linear fit from the time series (of duration 200 days centered on each sample except at the edges where the fit became one-sided and 100 days duration). Detrending is necessary because events in $\dot\nu$ dominate the long-term behavior, as discussed below, and tend to swamp the events in v visually. The $\delta\dot\nu(t)$ curves have not been detrended; therefore the slope of the *plotted* $\delta v(t)$ is not the same as the plotted $\delta\dot\nu(t)$. Figure 12 shows $\delta v(t)$ both before and after detrending.

Figures 12–17 show a rich variety of structure in δv and especially $\delta\dot\nu$. The overall level of activity is different in the
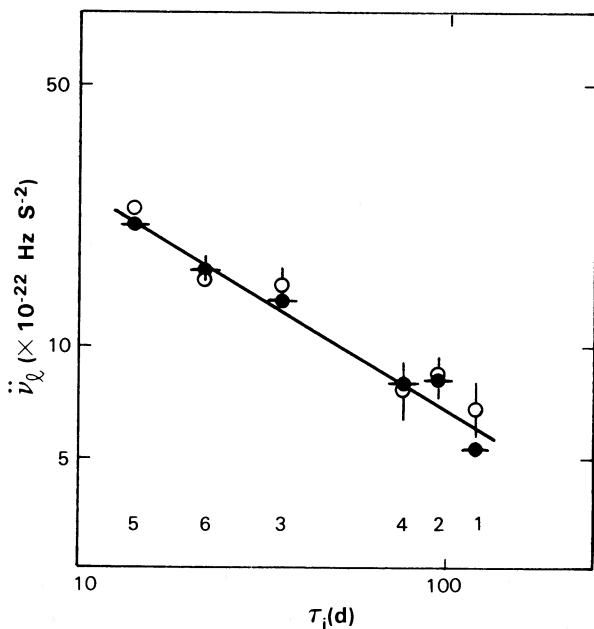

FIG. 11.—Log-log plot of $\ddot\nu_l$ vs. τ_i. Numbers refer to the macrojump number. *Solid circles:* results of exponential model fits, including $\pm 2\,\sigma$ errors where significant. *Open circles:* values of $\ddot\nu_l$ from independent third-order fits. *Solid line:* least-squares linear fit to the solid circles.
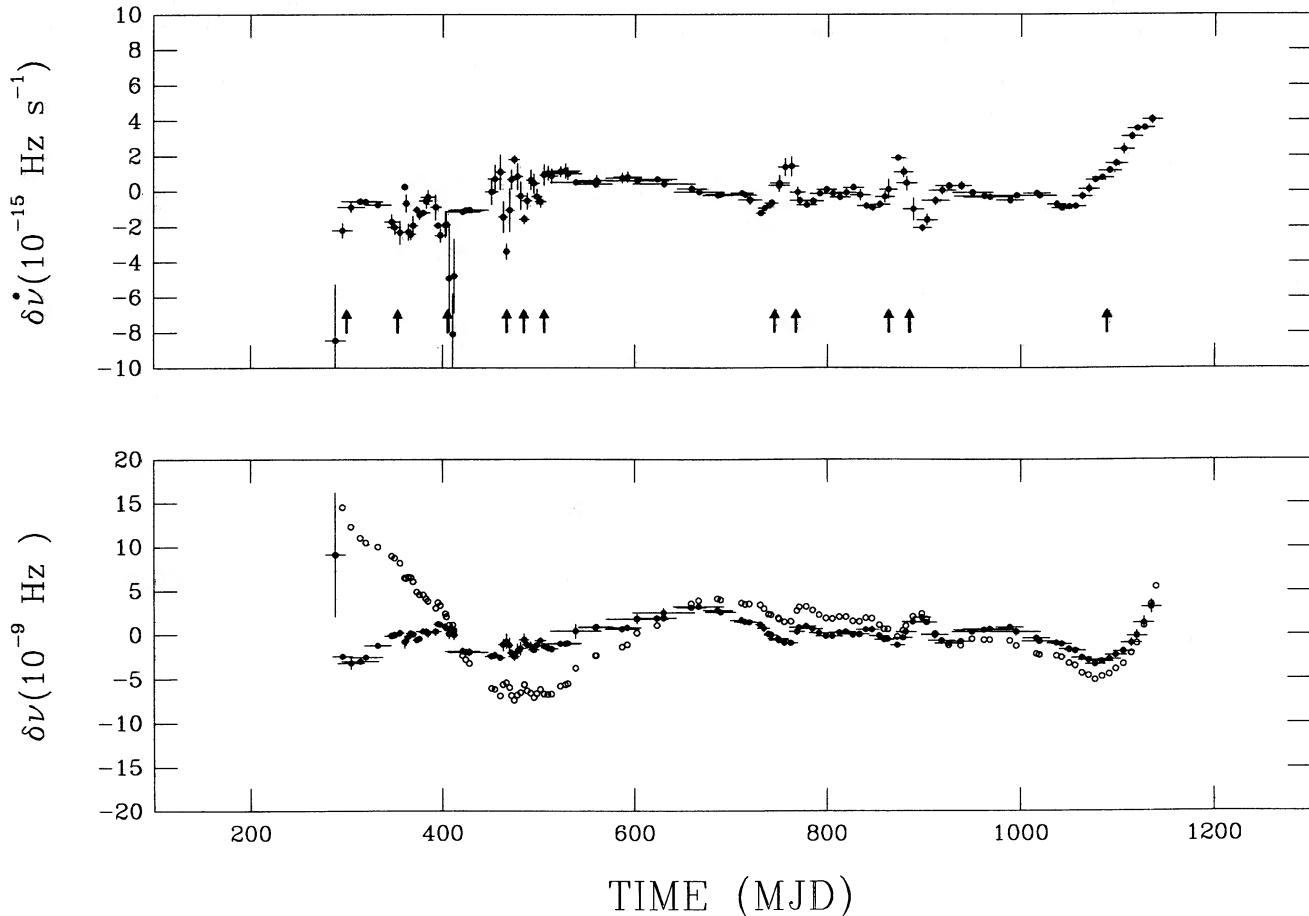
FIG. 12.—Interval between macrojumps 1 and 2. *Lower panel:* $\Delta v(t)$ from short polynomial fits before (*open circles*) and after (*solid circles*) detrending, as discussed in the text. *Upper panel:* $\Delta \dot{v}(t)$ from short polynomial fits. Vertical bars are $\pm 1 \ \sigma$ formal errors. Horizontal bars indicate the time interval for the polynomial fit. Vertical arrows indicate the epochs of candidate *microjump* events found from a threshold test described in the text.

different interjump intervals, the interval between jumps 1 and 2 (Fig. 12) being the quietest. Episodes of quiesence in $\delta \dot{v}$ (defined as contancy in the *slope* of $\delta \dot{v}$, $\delta \ddot{v}$) are rare. The longest interval of constant $\delta \ddot{v}$ is only 100 days, and the largest perturbations are $\sim 4 \times 10^{-15}$ Hz s^{-1} in ~ 12 days. Therefore, it is clear that the star is almost always rotationally active. To survey the nature of this activity, we first consider the phase residuals in statistical terms and then identify the forms of individual perturbations in $\dot{v}$.

a) Scaling Laws of Timing Noise

The simplest method for quantifying timing noise is to investigate the rms residual phase after performing least-squares fits of polynomials to the barycenric phase, as discussed in Paper III. A fit of an mth-order polynomial to $\delta \phi$ (the residual phase after removal of macrojumps) over a subinterval of length T yields an rms phase residual $\sigma_R(m, T)$, which receives contributions from *white noise* (measurement errors and other contributions that are uncorrelated over 1 day, such as scintillations and pulse phase jitter) and *timing noise* which is highly correlated from sample to sample. Thus $\sigma_R = (\sigma_{TN}^2 + \sigma_W^2)^{1/2}$. The white noise contribution may be estimated from phase differences of samples separated by less than $\Delta t_{max} = 0.2$ days, as discussed in Paper III (see eq. [12]). Restricting time separations in this fashion effectively filters out the correlated timing noise from the estimate; σ_W may then be quadratically sub-

tracted from σ_R to yield $\sigma_{TN}(m, T)$. Values of σ_W range from 20 to 30 μs.

Figure 18a shows $\sigma_{TN}(m = 3, T \approx 100$ days) as a function of time across the entire 14.5 yr of data. Vertical errors are based on the finite number of data points (see eq. [14] of Paper III). For comparison we also show (*open circles*) σ_{TN} as estimated for pseudo–white noise with the same amplitude as that of measurement errors in the pulsar data ($\sim 25 \ \mu$s). This demonstrates the reality of the excess phase residuals in the real data. The excess phase residuals quantified by σ_{TN} are highly variable, and there is no obvious evolution of σ_{TN} with time relative to the most recent macrojump. However, the *scatter* in values depends on the particular interjump interval, being smallest between jumps 1 and 2 and largest after jump 4.

To investigate the timing noise further, we performed a series of "octave fits" whereby each interval of length T_{max} between macrojumps was divided into $N_n = 2^n$ blocks of length $T_n = T_{max} 2^{-n}$ for $n = 0, 1, 2, 3$ (see Paper III). We do not fit across the macrojumps because, as stated before, there are unknown phase jumps at the macrojump epochs. In the following we designate the intervals between macrojumps as R_{12}, $R_{2'3}$, R_{34}, R_{45}, and R_{6+}, where we analyze data only after jump 2' for the second interval. The intervals R_{56} and R_{6+} are short and consequently only $n = 0, 1$ fits were performed.

Results are given in Table 4 where we tabulate σ_{TN} for octave fits of various length. We give results for third-order fits
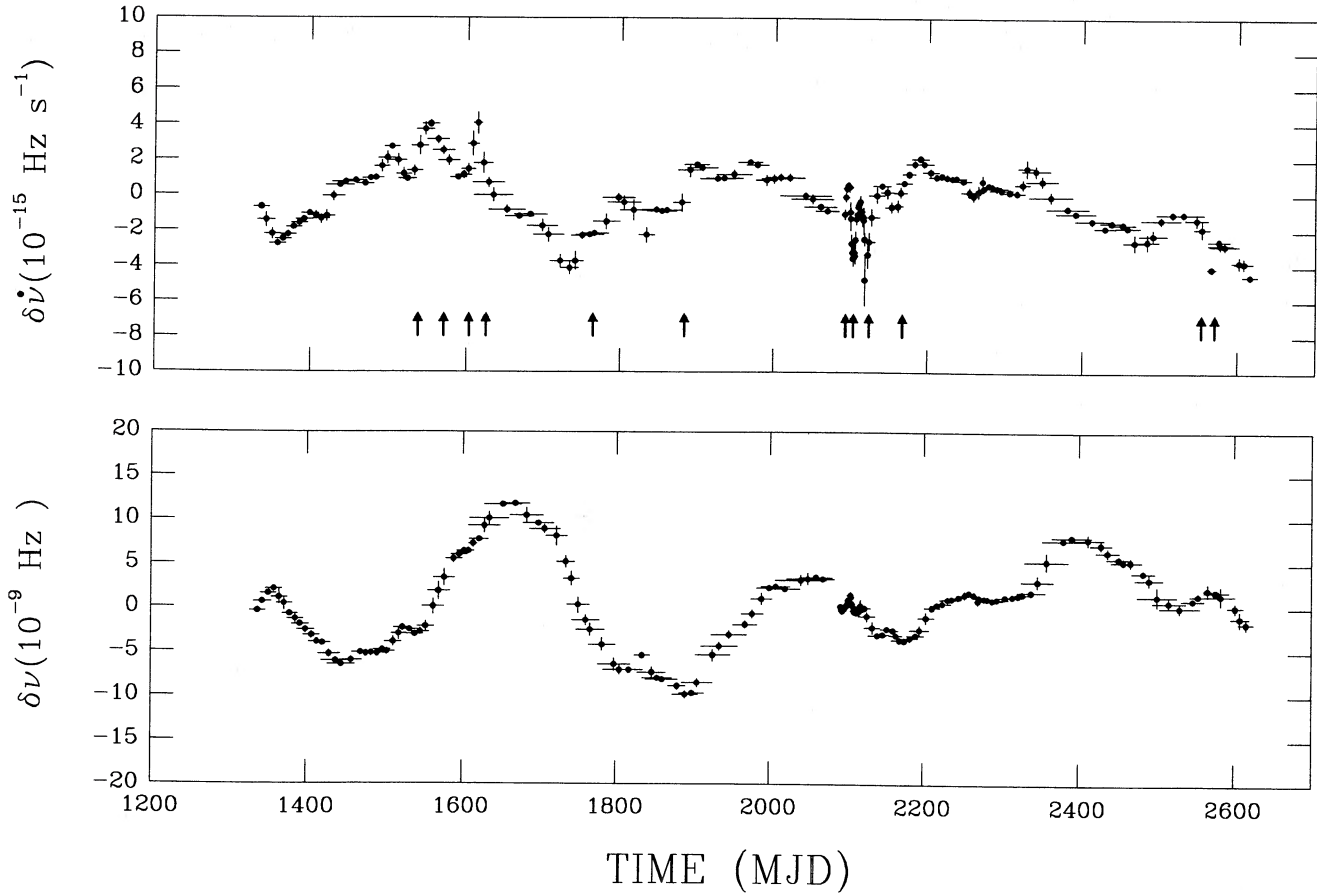
FIG. 13.—Interval between macrojumps 2′ and 3. *Lower panel:* Δν(t) from short polynomial fits and after detrending, as discussed in the text. *Upper panel:* Δν̇(t) from short polynomial fits. Vertical bars are ± 1 σ formal errors. Horizontal bars indicate the time interval for the polynomial fit. Vertical arrows indicate the epochs of candidate *microjump* events found from a threshold test described in the text.

($m = 3$) because they completely remove any contributions from a systematic ν̈. The mean, σ̄$_{TN}$, is simply the quadrature average of the N_n fits made for each octave. For $N_n \geq 2$ we also give the error in σ̄$_{TN}$, calculated as the rms scatter in individual values about the mean and divided by $N_n^{1/2}$. Figure 18b shows σ̄$_{TN}$ plotted against T_n. The remarkable features of this figure are as follows:

1. The timing noise is obviously nonstationary in that it grows as a positive power of T. [White noise only would yield σ$_{TN}$(3, T) independent of T].

2. The scaling of σ̄$_{TN}$ with T is roughly (from a visual estimate)

$$\bar{\sigma}_{TN} \approx \begin{cases} 0.32 \text{ ms } (T/300 \text{ days})^{1.5} & T \leq 300 \text{ days}, \\ 0.32 \text{ ms } (T/300 \text{ days})^{2.5} & T \geq 300 \text{ days}. \end{cases} \quad (7)$$

A formal least-squares fit to the points for $T \leq 250$ days yields an exponent of 1.6, while for $T \geq 250$ days, the exponent is 2.1. Although the uncertainties in the exponents are large, it is clear that steepening occurs.

3. The timing noise for $T \leq 300$ days is within a factor of 2 of being the same for all interjump intervals.

4. For large T (≥ 300 days), the scatter in σ̄$_{TN}$ becomes much larger.

b) Random Walk Processes

The scaling of σ̄$_{TN}$ with T is easily understood by considering the timing noise to result from small discontinuities in the

TABLE 4

TIMING NOISE VERSUS LENGTH OF FIT

| Interval	N_n	T_n (days)	σ̄$_{TN}$ (ms)
R_{12}	1	902	1.920
	2	445	0.480 ± 0.009
	4	215	0.145 ± 0.043
	7	108	0.074 ± 0.037
	16	48	0.020 ± 0.012
$R_{2'3}$	1	1341	5.340
	2	665	2.455 ± 0.258
	4	324	0.286 ± 0.039
	7	164	0.092 ± 0.012
	16	79	0.027 ± 0.003
R_{34}	1	975	12.000
	2	463	1.805 ± 0.011
	4	227	0.158 ± 0.028
	7	116	0.064 ± 0.008
	14	54	0.013 ± 0.005
R_{45}	1	1153	7.450
	2	568	2.320 ± 0.092
	4	277	0.446 ± 0.039
	8	134	0.088 ± 0.010
	15	69	0.039 ± 0.006
R_{56}	1	183	0.163
	2	80	0.047 ± 0.008
R_{6+}	1	176	0.246
	2	85	0.055 ± 0.010
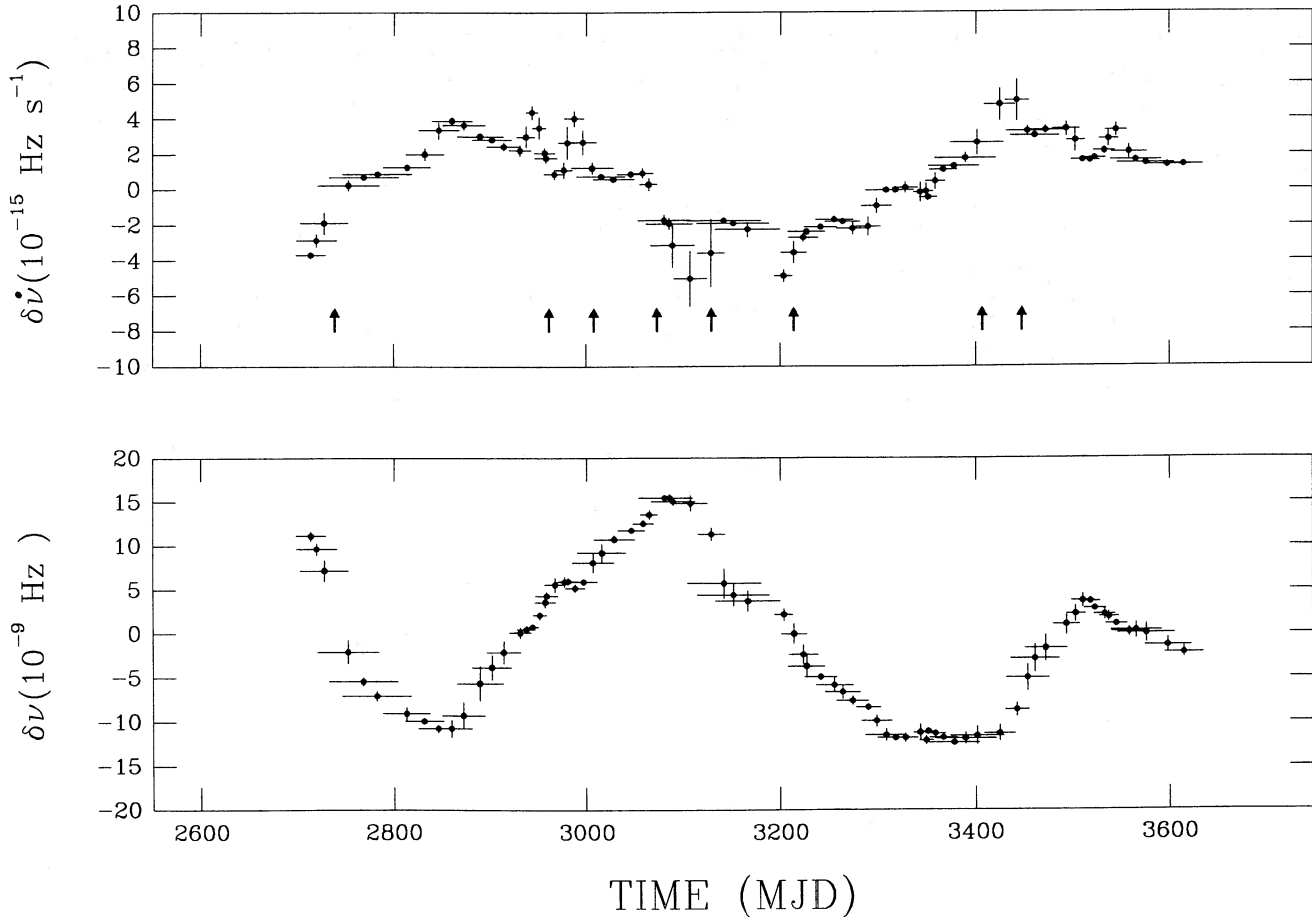
FIG. 14.—Interval between macrojumps 3 and 4. *Lower panel:* $\Delta v(t)$ from short polynomial fits and after detrending, as discussed in the text. *Upper panel:* $\Delta \dot{v}(t)$ from short polynomial fits. Vertical bars are $\pm 1\,\sigma$ formal errors. Horizontal bars indicate the time interval for the polynomial fit. Vertical arrows indicate the epochs of candidate *microjump* events found from a threshold test described in the text.

spin frequency and its derivative. In Paper III and elsewhere we have defined random walk processes in v and $\dot{v}$ that comprise an ensemble of many small step functions in v and $\dot{v}$, respectively. Each process, when integrated the appropriate number of times, yields a kth-order random walk in the phase (see Paper III), where $k = 1$ for step functions in v and $k = 2$ for step functions in $\dot{v}$. We refer to these, for later simplicity, as "frequency noise" (FN), and "spin-down noise" (SN). The phase variance produced by each process individually over a time span T is (in the continuum limit or for uniform sampling with a large number of samples)

$$\sigma_\phi^2(T) = \begin{cases} \frac{1}{12}S_1 T^3 & \text{FN} , \\ \frac{1}{120}S_2 T^5 & \text{SN} . \end{cases} \qquad (8)$$

Strength parameters are defined as

$$S_1 \equiv R\,\Delta v_{\rm rms}^2 , \qquad S_2 \equiv R\,\Delta \dot{v}_{\rm rms}^2 , \qquad (9)$$

where R is the step rate and the rms quantities refer to the amplitude distributions of individual events. We do not include macrojumps in these distributions.

An admixture of FN and SN yields a phase variance that is the sum of the variances if the two processes are statistically independent, which will hold if the events in Δv and $\Delta \dot{v}$ occur at independent times or if the amplitudes are uncorrelated. As discussed below, the data support this model, rather than one

in which FN and SN events occur together with correlated amplitudes. Therefore, we use the "uncorrelated" admixture model to interpret Figure 18b.

Although the total mean square phase is the sum of the variances of FN and SN in equation (8), the *measurable* timing noise [e.g., $\sigma_{\rm TN}(m, T)$] is not. This difference arises because an mth-order polynomial removes a larger fraction of SN than FN as a consequence of the two processes having different power spectra (actually, in this case, they have different amplitudes of polynomial components). Therefore we model the phase residual variance as

$$\sigma_{\rm TN}^2(m, T) = \frac{1}{12}C_{1,m}^{-2} S_1 T^3 + \frac{1}{120}C_{2,m}^{-2} S_2 T^5 , \qquad (10)$$

where $C_{k,m}$ are factors accounting for the effects of the fit. These are estimated in Cordes (1980) for $k = 1, 2$ and are (for $m = 3$) $C_{1,3} \approx 27$, $C_{2,3} \approx 72$.

The scaling of $\sigma_{\rm TN}$ in Figure 18b therefore suggests that Δv events dominate the phase for $T \le T_x \approx 300$ days, while $\Delta \dot{v}$ events dominate for $T \ge T_x$ days. Assuming that the two kinds of events have the same rate R, this requires that

$$\Delta \dot{v}_{\rm rms} \approx \frac{(10)^{1/2} C_{2,3}\,\Delta v_{\rm rms}}{C_{1,3}\,T_x} . \qquad (11)$$

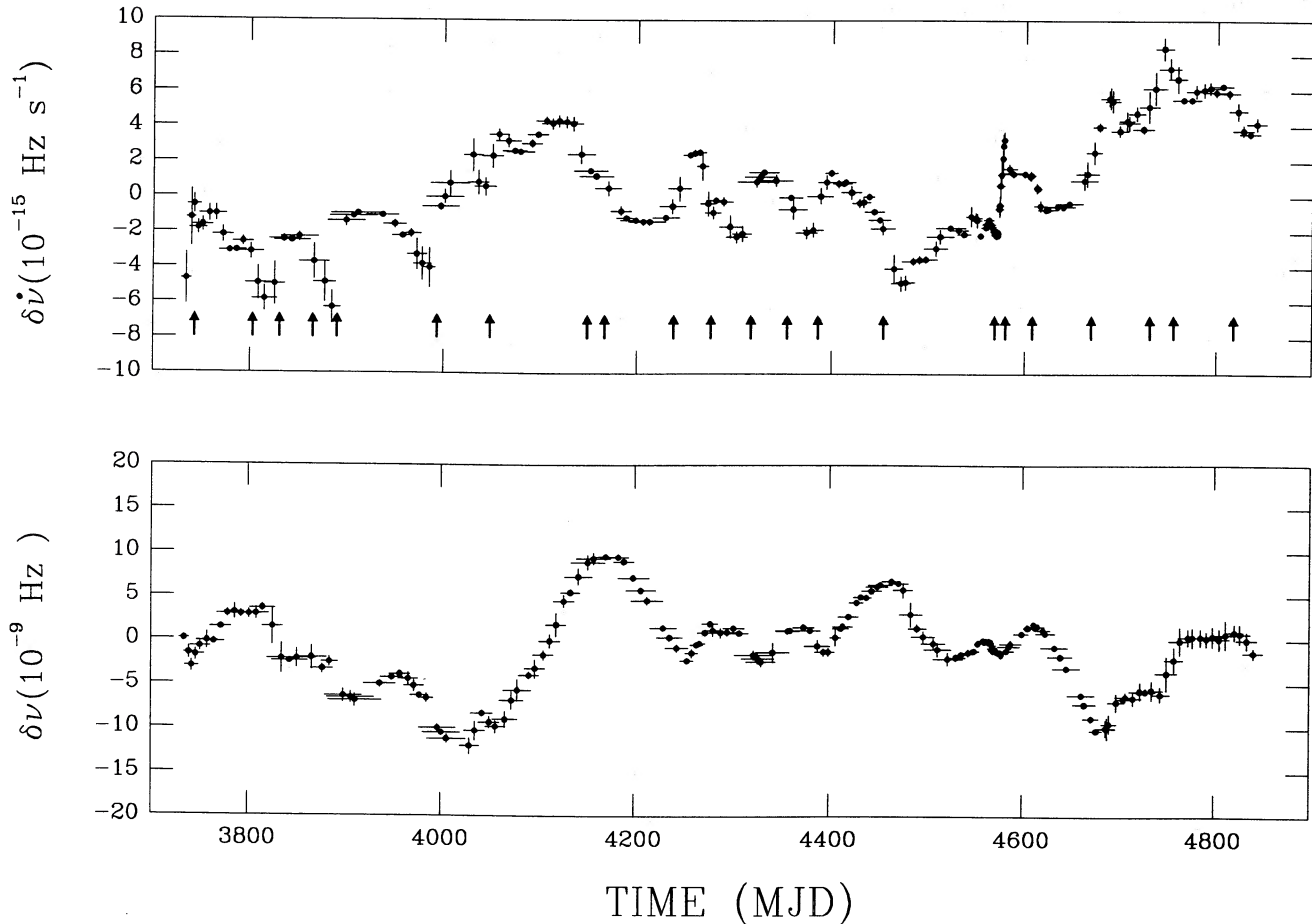In the analysis below, events are found with $\delta v \approx 10^{-8.3}$ Hz

FIG. 15.—Interval between macrojumps 4 and 5. *Lower panel:* $\Delta\nu(t)$ from short polynomial fits and after detrending, as discussed in the text. *Upper panel:* $\Delta\dot\nu(t)$ from short polynomial fits. Vertical bars are $\pm 1\,\sigma$ formal errors. Horizontal bars indicate the time interval for the polynomial fit. Vertical arrows indicate the epochs of candidate *microjump* events found from a threshold test described in the text.

which require $\delta\dot\nu \approx 10^{-14.7}$ Hz s^{-1}, as is consistent with actual events.

c) Identification of Microjumps

We identify and establish the significance of specific events in ν and its derivatives comparing by the observed amplitudes with random walk processes formed from very frequent events with amplitudes much too small to detect individually. Realizations of such processes (e.g., Fig. 13 of Paper III) show that spurious events which are produced by the combined effects of many small events can be identified by eye. For the FN and SN processes defined above, the differences $\delta\nu(\delta t) \equiv \nu(t + \delta t) - \nu(t)$ and $\delta\dot\nu(\delta t) \equiv \dot\nu(t + \delta t) - \dot\nu(t)$ are Gaussian random variables with standard deviations $\sigma_{\delta\nu} = (S_1 \delta t)^{1/2}$ and $\sigma_{\delta\dot\nu} = (S_2 \delta t)^{1/2}$, respectively, so long as $R\delta t \gg 1$. Consequently, a reasonable test is to compare candidate event amplitudes with these standard deviations.

Consider the sole occurrence of a random walk in $\dot\nu$ and that $\dot\nu(t)$ has been obtained by numerical differentiation of the phase. How small must the rate R be in order that events can be recognized? If all events have the same amplitude and if the amplitude is required to be larger than $N\sigma_{\delta\dot\nu}$ to be considered real, then the rate must satisfy $R^{-1} \gtrsim N^2\delta t$, where we have made use of the definition of S_2 above. For $\delta t = $ one sample interval ≈ 1 week, the constraint is $R^{-1} \gtrsim 63$ days for $N = 3$. Another requirement is that the contribution of white noise to

the errors in ν and $\dot\nu$ must also be small. In general, the errors in estimating $\delta\dot\nu$ seem to be dominated by the events themselves rather than by measurement errors.

To perform significance tests on individual events in $\delta\dot\nu$, we estimated the strength parameter S_2 for $\dot\nu$ events, defined the rms difference $\sigma_{\delta\dot\nu} = (S_2\,\delta t)^{1/2}$ appropriate for a large rate process, and numerically tested the difference $|\delta\dot\nu(\delta t)|$ against $N\sigma_{\delta\dot\nu}$, with $N = 3$. This test is less stringent than what we used in Paper III for other objects in the JPL sample, but for those objects measurement errors were considerably larger and were accounted for by requiring $N = 5$. Since the writing of Paper III, we have performed numerical experiments on simulated random walks which indicate that an $N = 3$ test finds very few spurious events.

In Figures 12–17 we indicate with arrows the epochs at which $\delta\dot\nu(\delta t)$ formally passes the 3 σ test. It is clear that some of these are due to bonafide step functions in $\dot\nu$, while some (recognized as a close pair of arrows indicating a positive fluctuation followed by a negative one, or vice versa) are pulses in $\dot\nu$ (step functions in ν). In some cases, only the rise or decay of the pulse passes the test, owing to the vagaries of sampling. In still other cases, events appear to be a combination of a pulse and a step.

We summarize the results of significance tests in Table 5, which lists the epoch, duration (actually an upper limit), amplitude, and type of event. For cases where a pulse occurs, we
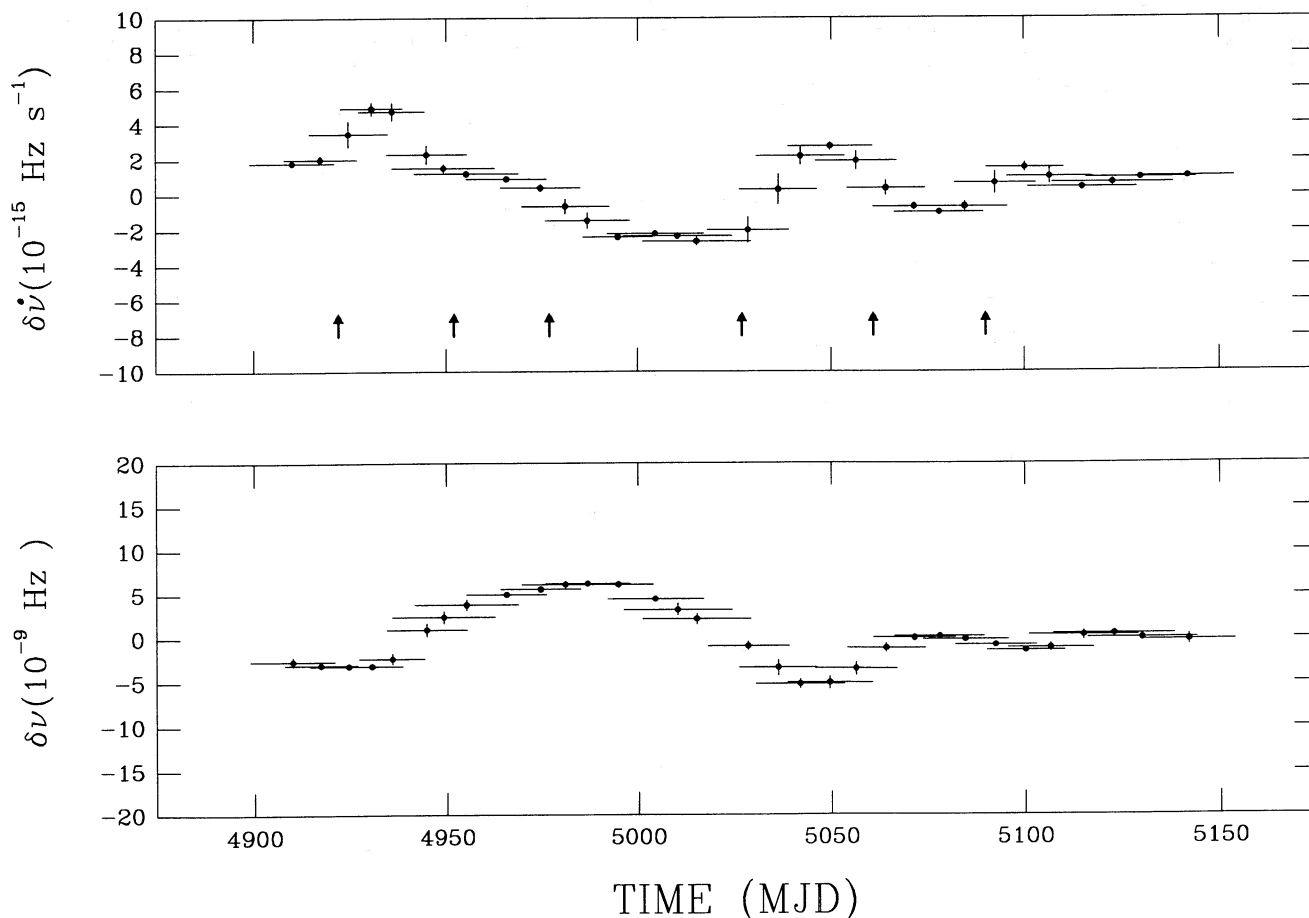
FIG. 16.—Interval between macrojumps 5 and 6. *Lower panel:* $\Delta\nu(t)$ from short polynomial fits and after detrending, as discussed in the text. *Upper panel:* $\Delta\dot{\nu}(t)$ from short polynomial fits. Vertical bars are $\pm 1\,\sigma$ formal errors. Horizontal bars indicate the time interval for the polynomial fit. Vertical arrows indicate the epochs of candidate *microjump* events found from a threshold test described in the text.

designate using L and T whether the leading or trailing edge of the pulse is identified and subscripts u and d are used to designate whether the fluctuation is upward or downward going. In some cases, we were unable to classify the type of event. Of the 19 step functions, 11 have positive amplitudes. Of the ~ 25 pulses, 15 have positive amplitudes.

d) Forms of Particular Microevents

The events that pass the threshold test show the following forms: positive and negative pulses in $\delta\nu$, positive and negative step functions in $\delta\dot{\nu}$, and unclassifiable events. Figures 19a and 19b show expanded portions of Figures 13 and 15 which are particularly good examples of prototype events that are superpositions of a pulse and a step function in $\delta\nu$. Similar superpositions may be seen in Figures 12–17, some of them negative going (as identified in Table 5). Still others show only a pulse or a step in $\delta\nu$.

These variations in apparent microjump form suggest that if each is characterized by amplitudes $\Delta\nu$ and $\Delta\dot{\nu}$ then the ratio $\Delta\nu/\Delta\dot{\nu}$ varies by much more than does the same ratio for macrojumps. This may be seen visually in Figure 20, which shows $\Delta\dot{\nu}$ plotted against $\Delta\nu$ for macrojumps and microjumps. It is obvious that the ratio varies by many orders of magnitude between the two kinds of jumps. The figure underscores the fact that macrojump 2' is intermediate in its parameters between the other macrojumps and microjumps.

In addition to pulse and step functions seen in $\delta\nu$, *ramp* functions also sometimes appear. However, it is not clear if these are real or whether they are produced by the fortuitous superposition of other kinds of events. For example, there appears to be an apparent slope change in $\delta\nu$ at MJD ~ 1050 (Fig. 12). This may be due to a true ramp event or it may be a succession of steps having the same sign. There appear to be episodes where a sequence of pulses and steps having the same sense may occur over the course of ~ 200 days. An example is the span from MJD ~ 2700–3050 where events seem to be positive going, while for the next ~ 200 days the events are negative going.

As discussed below, whatever the nature of the events, it seems that the star attempts to achieve a rotational steady state after a macrojump through discrete (micro)-perturbations and fails to do so in any convergent sense. The main evidence for the lack of convergence is that microjump activity in $\dot{\nu}$ has the same strength throughout each postmacrojump interval.

e) Relative Contributions of Macrojumps and Microjumps

Microjumps, although much smaller in amplitude than macrojumps, are sufficiently numerous that they contribute roughly the same amount to variations in rotational phase as do the macrojumps. Ignoring the linear and quadratic phase variations in the postmacrojump decay, the phase accumulation is roughly $\dot{\nu}_i\tau_i^2$ and is typically a few cycles. For micro-
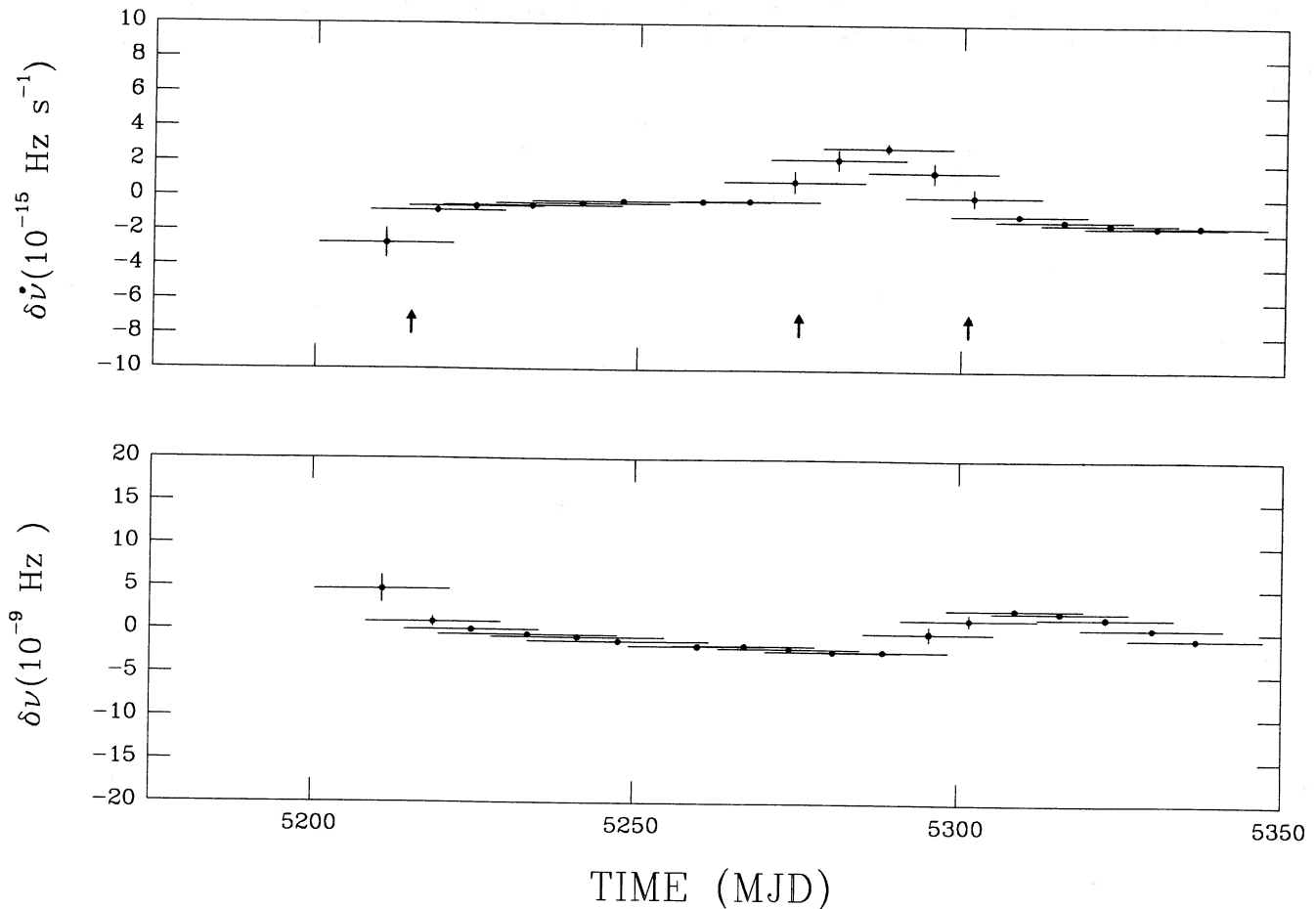
FIG. 17.—Interval after macrojump 6. *Lower panel:* $\Delta\nu(t)$ from short polynomial fits and after detrending, as discussed in the text. *Upper panel:* $\Delta\dot\nu(t)$ from short polynomial fits. Vertical bars are ± 1 σ formal errors. Horizontal bars indicate the time interval for the polynomial fit. Vertical arrows indicate the epochs of candidate *microjump* events found from a threshold test described in the text.

jumps, we use the scaling in equation (7) for $T \geq 300$ days to estimate for $T = 1000$ days a similar amount of random phase (when corrected by the factor $C_{2,3}$ that accounts for the effects of a least-squares fit). A similar consideration of fluctuations in $\dot\nu$ leads to the same conclusion that microjumps and macrojumps contribute roughly equally to the departures of the spindown from that expected for a simple torque mechanism. We note, however, that the amount of phase associated with the linear decay in $\dot\nu$ is at least 10 times larger than the microjump phase or the phase associated with the intermediate decay.

IV. ROTATION PHYSICS

Models for macrojumps have evolved considerably since the first macrojump from the Vela pulsar was seen in 1969. Initially, it was thought that a macrojump represented a moment of inertia change satisfying $\Delta I/I = -\Delta\nu/\nu$ and resulting from a decrease in rotation induced oblateness of the crust (or possibly an interior solid core). It was realized—after the second Vela macrojump occurred only 2 years after the first—that such models failed, even for the most extreme equations of state of nuclear matter (Pines and Shaham 1972). The fundamental problem with crustquake and corequake models is that the rotational oblateness is far too small to allow moment of inertia decrements of the implied amplitude at the observed rate. Although another explanation for macrojumps had to be found, a major success of the early model was the conclusion

that superfluidity was responsible for the long decay times (days) after the macrojumps (Baym et al. 1969).

Recent models (Alpar et al. 1984a, b) focus on the superfluid as the source for all discontinuities and decays and appear to have the same complexity as is exhibited in the macrojump data. In the following we summarize the model of Alpar et al. and briefly discuss the implications of our macrojump results in terms of the superfluid model. We conclude that the model is successful in describing macrojumps and that the radius where catastrophic unpinning events occur must vary significantly from one macrojump to the next.

We also consider microjumps in terms of the superfluid model and quake models, following the lead of Alpar, Nandkumar, and Pines (1986), and conclude that neither model, by itself, can cause the observed microactivity. However, crustquakes could conceivably trigger superfluid fluctuations and produce the observed kinds of microjumps so long as crustquakes produce moment of inertia changes that are both positive and negative.

a) Summary of Superfluid Vortex Models

Alpar et al. (1984a) discuss a model where the torque on the neutron star crust from the external magnetosphere is augmented with time variable internal torques from superfluid components. The basic features of the model are as follows:

1. Rotation tends toward a quasi–steady state wherein the
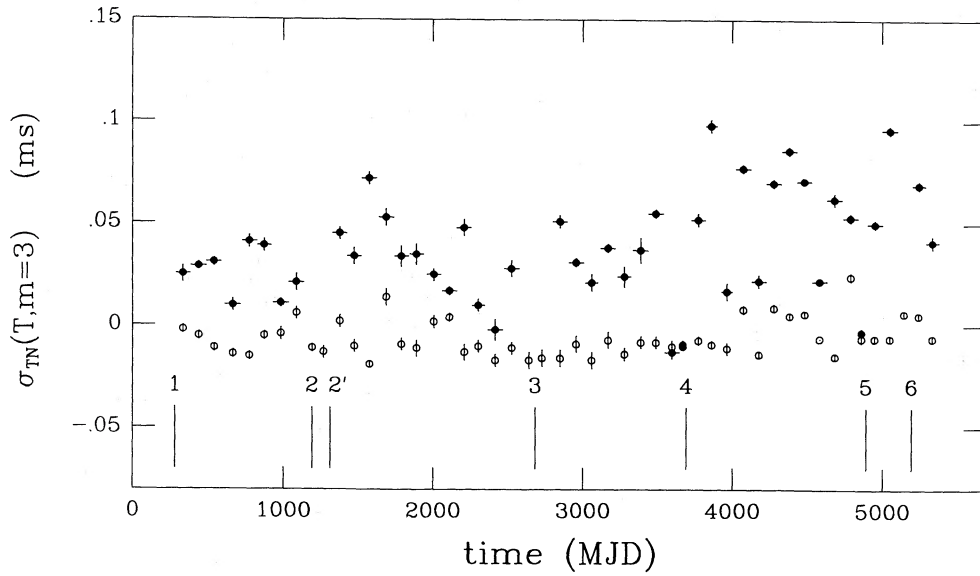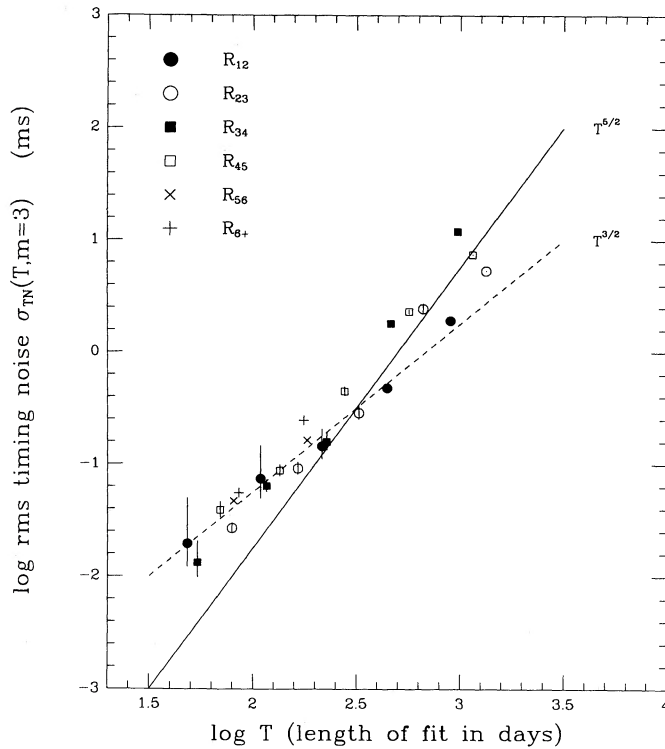
FIG. 18a

FIG. 18b

FIG. 18.—(a) (Solid circles) Excess phase residual $\sigma_{TN}(3, T)$ vs. time from nonoverlapping third-order polynomial fits after removal of the spin-down and macrojump model described in § II. Horizontal bars designate the extent of the fit ($T \sim 100$ days), and vertical bars are $\pm 1\ \sigma$ errors. None of the fits span the macrojumps. (Open circles) Excess residual for a simulation with white noise sampled at the same times as actual data and having a standard deviation of 25 μs. (b) Excess rms phase residual $\sigma_{TN}(3, T)$ vs. data block length T for third-order polynomial fits for the different postmacrojump regions.

crust angular velocity Ω_c smoothly decreases at a rate $\dot{\Omega}_c$. (In this section our discussion uses $\Omega \equiv 2\pi\nu$ and its derivatives for consistency with the work of Alpar et al. and because of its utility in discussing the physics.) The core superfluid is rigidly locked to the crust (coupling time of a few seconds), while superfluid components that permeate the crust are less strongly coupled. Given sufficient time the crustal superfluid components will also achieve a quasi-steady state configuration

$\Omega = \dot{\Omega}_c$, but having an angular velocity that is slightly larger than Ω_c. It is not clear whether all components of the Vela pulsar reach a quasi-steady state condition. If so, then $I\dot{\Omega}_c = N_{ext}$, where N_{ext} is the external torque and I is the total moment of inertia. If not, then the equation $I'(t)\dot{\Omega}_c = N_{ext}$ holds where $I'(t) \leq I$.

2. Superfluid components mimic the spin of ordinary fluid components through the presence of an array of quantized

TABLE 5

MICROACTIVITY IN $\dot{v}$

Macrojump Region	Epoch (MJD)	δt (days)	$\delta\dot{v}^a$	Sigma	Type of Event
R_{12}	300	24	7.5	10.1	Step
	353	13	2.0	3.3	Pulse (Lu)[b]
	405	13	−2.9	7.1	Pulse (Td)
	467	12	0.3	6.0	?
	485	26	1.9	4.1	?
	506	7	1.6	3.5	?
	745	18	2.3	3.2	Pulse (Lu)
	767	9	−1.9	3.6	Pulse (Td)
	864	16	2.4	3.5	Pulse (Lu?)
	885	17	−2.8	4.0	Pulse (Ld?)
$R_{2'3}$	1538	18	2.5	3.5	Pulse (Lu)
	1571	35	−3.0	3.0	Pulse (Td)
	1604	16	2.6	3.8	Pulse (Lu)
	1626	29	−3.6	4.4	Pulse (Td)
	1765	63	4.0	3.0	Step (?)
	1884	10	1.8	3.3	Step
	2095	26	−2.4	3.7	?
	2105	14	−2.0	5.4	?
	2125	26	2.1	4.7	?
	2168	39	3.2	3.1	Step + pulse (Lu)
	2554	22	−2.7	3.6	Pulse (Ld)
	2571	9	1.6	3.1	Pulse (Tu)
R_{34}	2740	48	3.9	3.4	Step
	2962	18	−1.1	3.9	Pulse (Td)
	3008	40	−3.2	3.3	Pulse (Td)
	3073	38	−4.3	4.1	Step
	3129	23	2.6	3.3	Pulse (Tu)
	3214	23	2.5	3.1	Pulse (Tu)
	3407	35	3.0	3.1	?
	3448	10	−1.7	3.2	?
R_{45}	3743	17	3.5	5.4	Step
	3803	17	−2.6	3.9	Pulse (Ld)
	3831	22	3.0	3.9	Pulse (Tu)
	3865	33	−3.4	3.5	Pulse (Ld)
	3890	21	3.6	5.2	Pulse (Tu)
	3993	42	3.8	3.9	Pulse (Tu)
	4048	16	2.5	3.8	?
	4149	45	−4.1	3.7	Step
	4167	59	−4.6	3.5	Step
	4238	37	3.6	3.7	Pulse (Lu)
	4276	28	−3.5	4.1	Pulse (Td)
	4317	25	3.3	4.0	Step
	4354	37	−3.2	3.2	Pulse (Ld)?
	4386	17	2.7	3.9	Pulse (Tu)?
	4454	34	−4.0	4.2	Step + pulse (Ld)?
	4569	19	3.5	4.9	Step
	4580	19	3.0	5.7	Pulse (Lu)
	4608	24	−2.4	3.1	Step
	4670	45	4.7	4.3	Step + pulse (Lu)
	4731	25	3.6	4.4	Pulse (Lu)
	4756	23	−2.9	3.6	Pulse (Ld)
	4818	21	−2.4	3.2	Step (d)
R_{56}	4922	16	2.6	3.9	Pulse (Lu)
	4952	42	−4.9	4.6	Pulse (Ld)
	4977	45	−3.9	3.5	Step
	5027	37	4.3	4.4	?
	5061	21	2.9	3.8	?
	5090	18	2.4	3.3	Step?
R_{67}	5215	10	2.0	3.8	Step
	5275	19	2.6	3.6	Pulse (Lu)
	5301	32	−3.7	4.0	Pulse (Td) + step

[a] 10^{-15} Hz s^{-1}.

[b] For pulse events, L and T denote "leading" and "trailing" edge, while "u" and "d" denote "upward" or "downward" going.

vortices, each carrying vorticity $\kappa = h/2m_n$, where h is Planck's constant and $2m_n$ (twice the neutron mass) is the mass of a Cooper pair. The angular velocity of the superfluid as a function of radius is

$$\Omega(r) = \kappa r^{-2} \int_0^r dr' \, r' n(r') , \qquad (12)$$

where $n(r)$ is the areal density of vortices. The total number of vortices in the star $N \approx 2\pi R^2 \Omega_c/\kappa \approx 10^{17.3}$ for Vela.

3. Spin-down of the superfluid *requires* that vortices move radially outward from the spin axis. Vortex motion represents a transfer of *angular momentum* without an accompanying transfer of mass. In some superfluid components (e.g., the core component), this motion is thought to be continuous and according to the quasi–steady state condition $\dot{\Omega} = \dot{\Omega}_c$. In other regions, where vortices are pinned to crustal nuclei, vortex motion is due to thermally induced creep. In regions where vortices cannot creep sufficiently fast, spin-down is effected in an *intermittent* fashion.

4. Macrojumps are spectacular examples of intermittent vortex motion, causing discontinuities $\Delta\Omega_c \equiv 2\pi \Delta v_c$ and $\Delta\dot{\Omega}_c \equiv 2\pi \Delta\dot{v}_c$ followed by "healing" of $\dot{\Omega}_c$ back to its prejump (or extrapolated) value. Discontinuities occur when the difference between superfluid and crustal angular velocities $\omega \equiv \Omega - \Omega_c$ exceeds a critical value ω_{cr} as a result of the spin-down. Physically this corresponds to the radial Magnus force exceeding the pinning force.

5. The discontinuity in Ω_c is the sudden transfer of angular momentum from unpinned vortices to the crust. If δN vortices unpin at a radius r_G and move to a radius $r_{G'} = r_G + \delta r_G$ with $\delta r_G \ll r_G$, then the fluid velocity between regions G and G' changes by an amount

$$\delta\Omega_B = -\frac{\kappa \, \delta N}{2\pi r_B^2} \qquad (13)$$

where $r_B = r_G + \delta r_G/2$. The observable discontinuity (of the crust) is

$$\Delta\Omega_c = \delta\Omega_B I_p/I_c , \qquad (14)$$

where I_p is the moment of inertia of the affected regions. The fraction of all vortices involved in a macrojump is $\delta N/N \approx \Delta\Omega_c \Omega_c/\Omega_c \Delta\dot{\Omega}_c \approx 10^{-4}$.

6. The spin-down rate changes by $\Delta\dot{\Omega}_c/|\dot{\Omega}_c| = -I_p/I_c$. The coupling of superfluid means that the moment of inertia I_c before the jump (which includes the crust, the strongly coupled core superfluid, and pinned superfluid components that satisfy the steady state condition) decreases to $I_c - I_p$.

7. Postmacrojump transients cause the superfluid rotation to tend toward quasi–steady state rotation. Alpar *et al.* (1984b) identify three superfluid components, each having an identifiable time scale. One is a "superweak" pinning component with $\tau_{sw} \approx 3$ days, the second is a "weak" pinning component with $\tau_w \approx 60$ days, and a third is the region between r_G and $r_{G'}$ which recouples on a time scale

$$t_B \approx \delta\Omega_B/\dot{\Omega}_c > 1600 \text{ days} . \qquad (15)$$

This last time scale exceeds all intervals between macrojumps, and therefore a linear torque is expected. The time scales τ_{sw} and τ_w are thought to correspond directly to those identified in our empirical model of § II—namely τ_s and τ_i—while the linear torque contributes to $\dot{v}_l$.
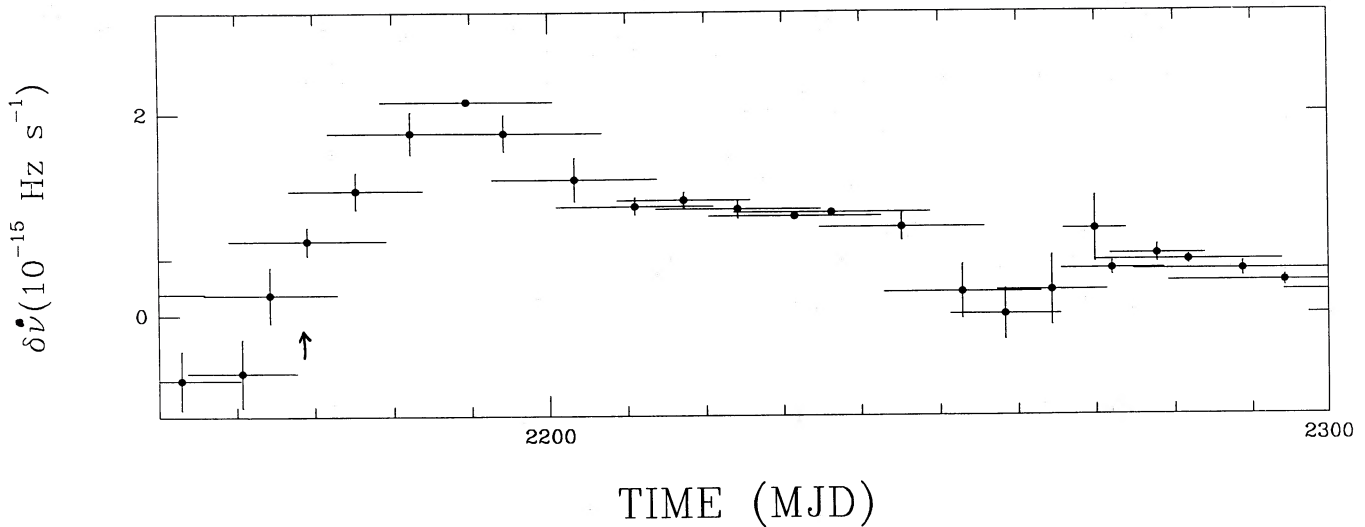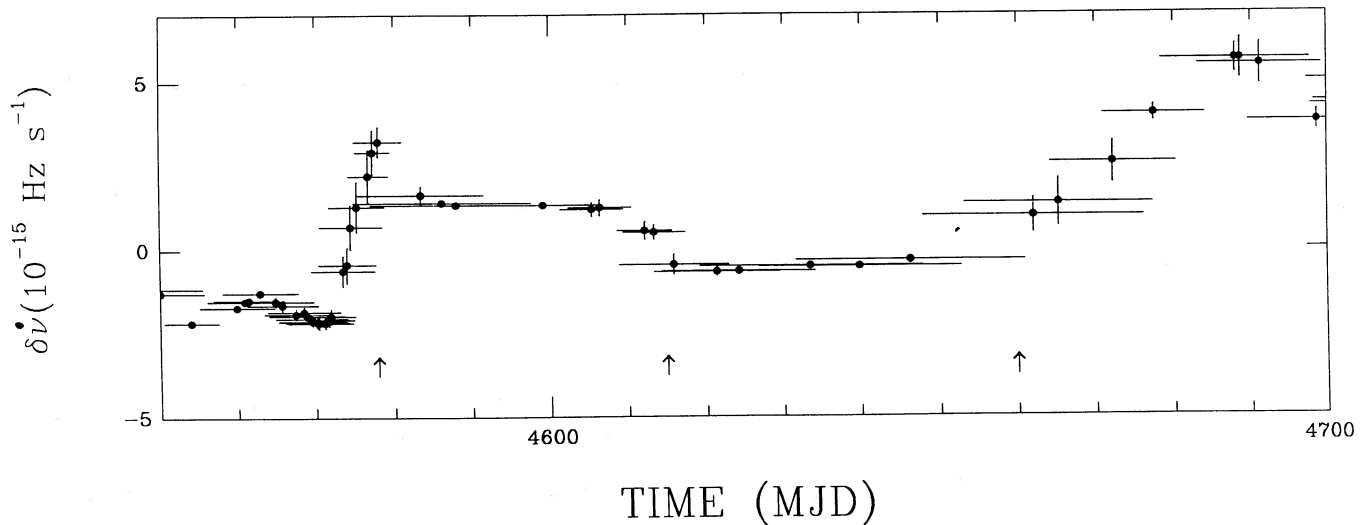
FIG. 19a

FIG. 19b

FIG. 19.—(a) Expanded portion of Fig. 13 showing a pulse + step function event in $\delta\dot{\nu}$. (b) Expanded portion of Fig. 15.

b) Comparison of Macrojumps with Superfluid Vortex Models

The macrojump model of Alpar et al. (1984a, b) accounts for most but not all of the observed features of macrojumps. The variability of macrojump parameters (Tables 1 and 2) implies that there is not a unique threshold for the occurrence of a macrojump, although the variation in jump amplitudes is only a factor of 2 (excluding jump 2′). The variations in the time constants τ_s and τ_i suggest there are significant variations in the radial locations at which vortices unpin/repin. In the model, the time constant for a given local region is

$$\tau = \left(\frac{kT}{r\kappa|\dot{\Omega}|}\right)\left(\frac{1}{\rho\xi b}\right), \tag{16}$$

where ρ is the mass density, r is the radial location, ξ is the radius of a vortex line, and b is the distance between pinning centers. The factor in the first pair of parentheses is unlikely to change by a factor of 2, while the second factor could easily change by a factor of 2 (or more) with a modest change in radius.

Indeed, Figure 6b of Alpar et al. 1984b shows the time constant of the weakly pinning component to decrease with decreasing density (increasing radius). The location in density of the regions of pinned vorticity apparently must change by a few times 10^{13} g cm^{-3} (a few tens of percent) to account for the observed variations. Using the equation of hydrostatic equilibrium (relativistic corrections are small), we estimate that the associated change in radius is

$$\frac{\delta r}{R} \approx \left(\frac{v_s}{c}\right)^2\left(\frac{R}{R_s}\right)\left(\frac{\delta\rho}{\rho}\right), \tag{17}$$

where v_s is the speed of sound in the relevant layer and $R_s \approx 4$ km is the Schwarzschild radius. For a relatively hard equation of state (e.g., Pandharipande, Pines, and Smith 1976; Shapiro and Teukolsky 1983), $\delta r \approx 10^{-2.7}R$, or a few times 10 m for $R = 10$ km.

Variations in the location of the unpinning/repinning region may also explain the observed anticorrelation of the intermediate time constant τ_i with the linear decay $\dot{\nu}_l$. In the Alpar et
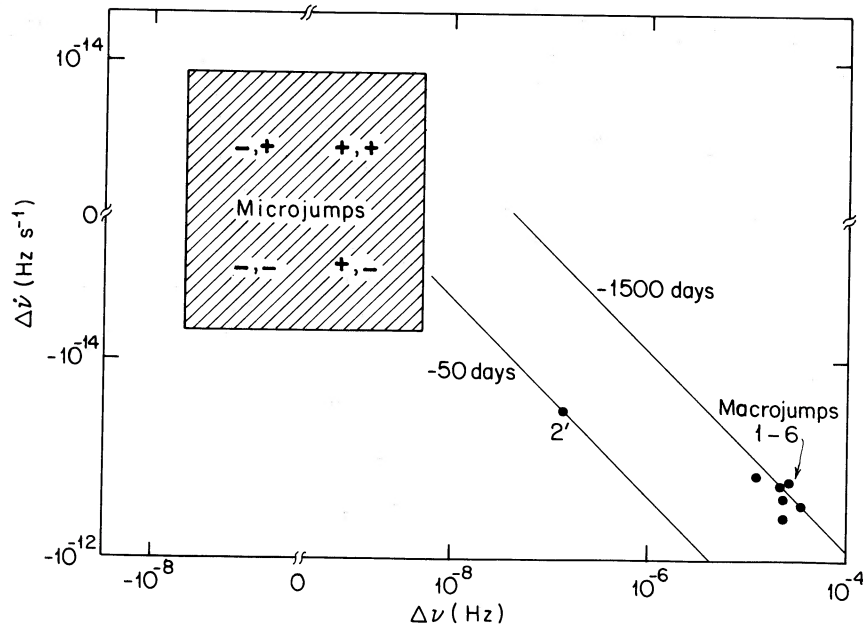
FIG. 20.—Comparison of macrojump and microjump events. Filled circles show $\Delta\dot{v}$ plotted against Δv for macrojumps. Light lines are loci of constant $\Delta v/\Delta\dot{v}$, equal to about -1500 days for macrojumps 1–6 and -50 days for macrojump 2′. Shaded square delineates the range of microjump parameters, with the four quadrants of the square labeled with the signs of $\Delta\dot{v}$ and Δv.

al. model, τ_i is associated with the weakly pinned component residing outside the glitch region (i.e., radius $> r_{G'}$), while the linear decay is caused by vortex recoupling in regions G and G'. The linear decay (described by the quantity $\ddot{v}_l$ in the data analysis) is given by

$$\ddot{\Omega}_{c_l} = \dot{\Omega}_c I_A/I_c \, t_B = \dot{\Omega}_c^2 I_A/I_c \, \delta\Omega_B \,, \tag{18}$$

where I_A is the combined moment of inertia of regions G and G' and τ_i is given as above for a region external to G'. An increase in I_A associated with a larger glitch region may correspond to the region exterior to G' being at a larger radius and characterized by a smaller τ_i.

Unfortunately, this picture encounters difficulty because a small radial change induces a change in $\ddot{\Omega}_{c_l}$ (via I_A) dominated by the change in density, not by the radial factors. This can be seen from the fact that $\ddot{\Omega}_{c_l} \propto \rho r^5$. For a TNI equation of state (Friedman and Pandharipande 1981), we estimate that the pinning region has a radial thickness of ~ 0.5 km for a 1.4 $M_\odot$ star with a radius 11 km. The change in radius accounts for only a 25% change in $\ddot{\Omega}_{c_l}$, while the density changes by an order of magnitude across the region. Therefore, the observed correlation $\ddot{\Omega}_{c_l} \propto \tau_i^{-0.6}$ implies that $\tau_i \propto \rho^{-1.7}$, in contrast to Figure 6b of Alpar *et al.* (1984b), which shows τ_i varying with a positive power of ρ. Formally, one could conclude that rather than corresponding to a region of weak pinning, the region responsible for τ_i comprises strong pinning, as in Figure 6a of Alpar *et al.* This conclusion contradicts Alpar *et al.* who concluded that pinning had to be weak on the basis of X-ray observations and vortex creep energy dissipation calculations. Further work in this area must await better microscopic calculations of the pinning parameters, a point already emphasized by Alpar *et al.* (1984b).

c) Microjump Models

The notable aspect of microjumps is that, whereas macrojumps have a well-defined signature $(\Delta\Omega_c, \Delta\dot{\Omega}_c) = (+, -)$, microjumps show a large range of structure and signatures.

Some of the variations seem to be resolved in time, but it is uncertain whether the apparent resolution represents a *rise time* of an event or a *decay time* after an event, because of the discrete sampling of the data.

Alpar, Nandkumar, and Pines (1986) have discussed microactivity for some two dozen pulsars, including Vela, in statistical terms by comparing power spectra of $\dot{\Omega}_c$ with those predicted from several models. They considered three basic models for microactivity:

Case 1: Microjumps are due *solely* to vortex unpinning events and are therefore qualitatively like miniature versions of macrojumps.

Case 2: Microjumps are mixed events, initiated by some process other than vortex unpinning, such as a crust quake, which then *induces* vortex unpinning.

Case 3: Microjumps are purely due to process(es) other than vortex unpinning.

In all three cases, the pinned superfluid produces a transient response to the microjump, regardless of the initial cause of the microjump. Alpar, Nandkumar, and Pines found that the microactivity of most pulsars could not be accounted for by for by case 1. There were pulsars for which cases 2 and 3 seemed to apply, and others for which the activity could not be accounted for if pinned regions have the same properties (e.g., time constants) as found in the Vela pulsar.

It is useful to consider the possible microjump signatures for the three cases. Since case 1 is essentially the same as a macrojump model, event signatures must be of the same form, namely $(\Delta\Omega_c, \Delta\dot{\Omega}_c) = (+, -)$. In case two, the discontinuity in Ω_c receives a contribution from both the cause of the event, say a moment of inertia change ΔI, and the unpinning event. Consequently, the net $\Delta\Omega_c$ can be $+$, $-$, or 0 (assuming ΔI can be $+$ or $-$) but will always be accompanied by a negative change in $\dot{\Omega}_c$, as in a macrojump, because the unpinning always reduces the moment of inertia acted upon by the external torque. Therefore the possible signatures for case 2 are $(\Delta\Omega_c, \Delta\dot{\Omega}_c) = (+, -), (-, -)$, and $(0, -)$. For cases 1 and 2, the post

microjump response is described by exponential response(s) with time constant(s) τ, as before, and the fraction of the jump in $\Delta\Omega_c$ that decays away is Q. For case 1, $Q \equiv 1$, whereas for case 2, $Q \geq 1$. For case 3, the superfluid is involved only as a response to the initial event. Alpar, Nandkumar, and Pines argue that the event decay has $Q = I_p/I_c \approx 10^{-2}$ and therefore the superfluid response is negligible. Consequently, the possible event signatures for case 3 are effectively $(\Delta\Omega_c, \Delta\dot{\Omega}_c) = (+, 0)$ and $(-, 0)$.

The observational results we have obtained on microjumps are apparently in conflict with the event signatures predicted for all three cases. That is, some of the events may be produced by the model described above, but the appearance of *positive* discontinuities in $\dot{\Omega}_c$ (or equivalently, $\dot{v}$ in the data analysis section of the paper) is in conflict with the expected signatures. Of course, the observed microjumps may only *apparently* show events of both signs. Suppose that all events in $\dot{\Omega}_c$ are negative going, followed by healing on some time scale τ. If the rate of such events R satisfies $R\tau \ll 1$ then events will be widely separated and the signature will be easy to discern. If $R\tau \sim 1$ (as observed), then *apparently* positive going pulses in Ω_c can be observed when an event in $\dot{\Omega}_c$ heals and another event occurs just after. Similarly an apparently negative going pulse in $\dot{\Omega}_c$ may appear from a negative going discontinuity followed by a rapid healing (i.e., $\tau \lesssim$ sample interval ≈ 7 days).

If positive discontinuities in $\dot{\Omega}_c$ actually occur, there must be some mechanism causing *increases* in moment of inertia that involve a *sudden*, coherent repinning of uncoupled vortices or there must be a way for vortices to move *inward* toward the spin axis. The distribution of vortices may be locally irregular, as suggested by Alpar *et al.*, so that motions of vortices on the local scale can run counter to the spatially and temporally averaged flow. If vortex motions are of importance in microjump discontinuities, then coherent action by $\delta N \approx N \Delta\Omega_c \dot{\Omega}_c / \Omega_c \Delta\dot{\Omega}_c \approx 10^{11}$ vortices is required.

It is worthwhile considering pure crustquake models for microjumps, because they can be rejected as the *sole* cause of microactivity. Moment of inertia discontinuities in the crustal component induce jumps satisfying

$$\frac{\Delta\Omega_c}{\Omega_c} = -\frac{\Delta\dot{\Omega}_c}{|\dot{\Omega}_c|} = -\frac{\Delta I_c}{I_c} . \tag{19}$$

Clearly, events involving moment of inertia changes produce fractional amplitudes of events that are anticorrelated. This model can be immediately rejected because the observed events satisfy

$$|\Delta\Omega_c|/\Omega_c \approx 10^{-5} |\Delta\dot{\Omega}_c/\dot{\Omega}_c| . \tag{20}$$

Therefore, the only possibility is that quakes produce discontinuities in Ω_c and that they possibly trigger events in $\dot{\Omega}_c$.

V. SUMMARY AND CONCLUSIONS

We have analyzed 14.5 yr of JPL timing data to study the spindown of the Vela pulsar. Discontinuities in the spin frequency and its derivatives have bimodal amplitude distributions. *Macrojumps* ("glitches") are characterized by relative changes in spin rate $\Delta v/v \sim 10^{-6}$ and derivative $\Delta\dot{v}/\dot{v} \sim 10^{-2}$, while *microjumps* have $|\Delta v/v| \lesssim 10^{-9}$ and $|\Delta\dot{v}/\dot{v}| \lesssim 10^{-4}$. Macrojumps display a signature $(\Delta v, \Delta\dot{v}) = (+, -)$ with a well-defined ratio of the amplitudes. Microjumps, however, show all possible signs of events and a large range in $\Delta v/\Delta\dot{v}$. The average interval between macrojumps is ~ 1000 days, while microjumps occur about once every 100 days.

Ten parameters are required to quantify each macrojump and the subsequent evolution of $\dot{v}$. The macrojump itself is described by three amplitudes Δv, $\Delta\dot{v}$, and $\Delta\ddot{v}$ and an epoch. The postjump evolution of $\dot{v}$, given by six parameters, consists of a short-term exponential decay (characterized by an amplitude $\dot{v}_s$ and decay time $\tau_s \sim 6$ day); an intermediate-term exponential decay (characterized by $\dot{v}_i$ and $\tau_i \sim 60$ day); and a linear decay (characterized by $\dot{v}_l$ and $\ddot{v}_l$ with $|\dot{v}_l|/|\ddot{v}_l| \sim 500$ yr). All 10 macrojump parameters vary significantly from jump to jump, suggesting that the threshold for occurrence of a macrojump varies within the star and/or with time. Furthermore, the linear decay parameter $\ddot{v}_l$ is highly negatively correlated (-94%) with the exponential parameter τ_i.

Microjumps are analogous to the "timing noise" that has been identified in most other pulsars. The arrival time measurements are sufficiently accurate to allow identification of individual discontinuities in v and its derivatives. Arrival times obtained at 2.4 GHz have a typical uncertainty of 25 μs. The weekly sampling of the data is sufficient to resolve different events, and some appear to have rise times ~ 5–20 days. Microjumps are typically combinations of step functions in v, $\dot{v}$, and possibly $\ddot{v}$. Microactivity occurs throughout the intervals between macrojumps. It appears stronger between some macrojumps than others, but has no obvious dependence on the elapsed time since the latest macrojump.

Some components of the star evidently fail to achieve a rotational steady state after a macrojump (if ever). The angular velocities of different components evolve through sequences of discrete microjumps rather than through smooth variations. In terms of superfluid vortex models, the variation in macrojump parameters and the correlation between $\ddot{v}_l$ and τ_i suggest that the location in density of the relevant region of pinned vorticity varies by some $\sim 10^{13}$ g cm^{-3}, corresponding to a radial change of tens of meters. The behavior of microjumps cannot be explained with models solely involving vortex unpinning or solely by moment of inertia changes associated with crustquakes or corequakes. Evidently, some combination of the two or additional mechanisms are required to explain microjumps fully. Some microactivity may be associated with sudden, coherent repinning events comprising $\delta N \approx 10^{11}$ vortices that counter the effects of sudden unpinning events of similar numbers of vortices.

APPENDIX A
CONVERSION OF PERIOD TO FREQUENCY

The rotation frequency v, the spin-down rate $\dot{v}$, and its derivative $\ddot{v}$ can be expressed concisely as functions of the pulsation period P and its derivatives $\dot{P}$ and $\ddot{P}$:

$$v = P^{-1} , \tag{A1}$$

$$\dot{v} = -P^{-2}\dot{P} , \tag{A2}$$

$$\ddot{v} = -P^{-2}\ddot{P} + 2P^{-3}\dot{P}^2 . \tag{A3}$$

Similarly, abrupt changes Δv, $\Delta \dot{v}$, and $\Delta \ddot{v}$ can be written in terms of the measured changes ΔP, $\Delta \dot{P}$, and $\Delta \ddot{P}$:

$$\Delta v = -P^{-2}\Delta P , \tag{A4}$$

$$\Delta \dot{v} = -P^{-2}\Delta \dot{P} + 2P^{-3}\dot{P}\Delta P , \tag{A5}$$

$$\Delta \ddot{v} = -P^{-2}\Delta \ddot{P} + 4P^{-3}\dot{P}\Delta \dot{P} + (2P^{-3}\ddot{P} - 6P^{-4}\dot{P}^2)\Delta P . \tag{A6}$$

The quantities ΔP, $\Delta \dot{P}$, and $\Delta \ddot{P}$ are measured for each jump, and by using nominal values of P, $\dot{P}$, and $\ddot{P}$ in the vicinity of the jump, we evaluate Δv, $\Delta \dot{v}$, and $\Delta \ddot{v}$ using equations (A4)–(A6).

Finally, dividing the changes of equations (A4)–(A6) by the corresponding nominal parameter values of equation (A1)–(A3), we compute the fractional changes $\Delta v/v$, etc., in terms of changes in the period parameters. Note that fractional changes in the rotational parameters are not precisely identical to the fractional changes in the period parameters:

$$\Delta v/v = -\Delta P/P , \tag{A7}$$

$$\Delta \dot{v}/\dot{v} = \Delta \dot{P}/\dot{P} - 2\Delta P/P , \tag{A8}$$

$$\Delta \ddot{v}/\ddot{v} = [\Delta \ddot{P}/\ddot{P} - 2\beta\Delta \dot{P}/\dot{P} - 2(1 - 3\beta/2)\Delta P/P](1 - \beta)^{-1} , \tag{A9}$$

where

$$\beta = 2\dot{P}^2/P\ddot{P} . \tag{A10}$$

Variations in β are caused mostly by changes in $\ddot{P}$. Since $|\ddot{P}| \geq 5 \times 10^{-24}$, we always have $|\beta| \leq 5 \times 10^{-2}$ for PSR 0833—45.

APPENDIX B
SELECTING PARAMETER VALUES

The difference between the measured phase $\phi_m(t)$ and the predicted phase $\phi(t)$ is the phase residual $\Delta\phi(t)$. Differentiating numerically $\Delta\phi(t)$ yields $\Delta v(t)$, the perturbed or unmodeled component of the spin rate. That is,

$$\Delta v(t) = \frac{\partial \Delta\phi(t)}{\partial t} . \tag{B1}$$

Concentrating for the moment on the intermediate and long-term components of the rotation, the unmodeled component becomes

$$\Delta v(t) = \Delta v_0 + (\dot{v}_0 + \Delta \dot{v}_i)t + \tfrac{1}{2}(\ddot{v}_0 + \Delta \ddot{v}_i)t^2 - \Delta(\dot{v}_i \tau_i)(1 - e^{-t/\tau_i}) . \tag{B2}$$

Each error (Δv_0, etc.) has its own characteristic signature. In particular, discrete events in v and $\dot{v}$ produce level shifts and slope changes, respectively. Plots of $\Delta v(t)$ were an aid in selecting τ_i and were indispensible in selecting values for the four parameters describing jump 2'.

If the pulsar timing data were free of all noise except *measurement* noise, then a perfect selection of the model parameters would yield phase residuals which, when plotted versus time, are distributed symmetrically about $\Delta v = 0$. Imagine, however, that one unmodeled event in $\dot{v}$ perturbs the $\Delta v(t)$ curve at some epoch in the data span. One or both linear segments of the curve will then be tilted relative to the $\Delta v = 0$ axis. Next allow an exponentially decaying jump such as 2' to occur in one segment, thus perturbing that segment from a straight line. If we choose the model of that perturbation and the values of its parameters correctly, the linear trend of that segment of $\Delta v(t)$ will be recovered.

It is toward this ideal that we have adjusted the model parameters to obtain a minimum perturbation from a straight, but not necessarily horizontal line. This aid was used in selecting parameter values for the intermediate-term decays, in the short-term decay following jump 2', and in assessing the errors in modeling the short-term decays.

REFERENCES

Alpar, M. A., Anderson, P. W., Pines, D., and Shaham, J. 1981, *Ap. J. (Letters)*, **249**, L29.
———. 1984a, *Ap. J.*, **276**, 325.
———. 1984b, *Ap. J.*, **278**, 791.
Alpar, M. A., Nandkumar, R., and Pines, D. 1986, *Ap. J.*, **311**, 197.
Armstrong, J. W. 1984, *Nature*, **307**, 527.
Arons, J. 1981, in *IAU Symposium 95, Pulsars*, ed. W. Sieber and R. Wielebinski (Dordrecht: Reidel), p. 69.
Backus, P. R., Taylor, J. H., and Damashek, M. 1982, *Ap. J. (Letters)*, **255**, L63.
Baym, G., Pethick, C., Pines, D., and Ruderman, M. 1969, *Nature*, **224**, 872.
Blandford, R. D., and Narayan, R. 1984, *M.N.R.A.S.*, **213**, 591.
Boynton, P. E., Groth, E. J., Hutchinson, D. P., Nanos, G. P., Jr., Partridge, R. B., and Wilkinson, D. T. 1972, *Ap. J.*, **175**, 217.
Cordes, J. M., and Downs, G. S. 1985, *Ap. J. Suppl.*, **59**, 343 (Paper III).
Cordes, J. M., and Greenstein, G. 1981, *Ap. J.*, **245**, 1060.
Cordes, J. M., and Helfand, D. J. 1980, *Ap. J.*, **239**, 640.
Cordes, J. M., Pidwerbetsky, A., and Lovelace, R. 1986, *Ap. J.*, **310**, 737.
Downs, G. S. 1981, *Ap. J.*, **249**, 687 (Paper I).
———. 1982, *Ap. J. (Letters)*, **257**, L67.
Downs, G. S., and Krause-Polstorff, J. 1986, *Ap. J. Suppl.*, **62**, 81 (Paper IV).
Downs, G. S., and Reichley, P. E. 1983, *Ap. J. Suppl.*, **53**, 169 (Paper II).
Friedman, B., and Pandharipande, V. R. 1981, *Nucl. Phys. A*, **361**, 502.
Groth, E. J. 1975, *Ap. J. Suppl.*, **29**, 453.
Hamilton, P. A., McCulloch, P. M., and Royle, G. W. R. 1982, *IAU Circ.*, No. 3729.

Klekocink, A. R., McCulloch, P. M., and Hamilton, P. A. 1985, *IAU Circ.*, No. 4089.
Lyne, A. G. 1987, *Nature*, **326**, 569.
Manchester, R. N. 1981, in *IAU Symposium 95, Pulsars*, ed. W. Sieber and R. Wielebinski (Dordrecht: Reidel), p. 267.
Manchester, R. N., Goss, W. M., and Hamilton, P. A. 1976, *Nature*, **259**, 291.
Manchester, R. N., and Taylor, J. H. 1977, *Pulsars* (San Francisco: Freeman).
Manchester, R. N., *et al.* 1978, *M.N.R.A.S.*, **184**, 159.
McCulloch, P. M. 1986, private communication.
McCulloch, P. M., Hamilton, P. A., Royle, G. W. R., and Manchester, R. N. 1981, *IAU Circ.* No. 3644.
———. 1983, *Nature*, **302**, 319.
Pandharipande, V. R., Pines, D., and Smith, R. A. 1976, *Ap. J.*, **208**, 550.
Pines, D., and Shaham, J. 1972, *Nature Phys. Sci.*, **235**, 43.
Radhakrishnan, V., and Manchester, R. N. 1969, *Nature*, **222**, 228.
Reichley, P. E., and Downs, G. S. 1969, *Nature*, **222**, 229.
Rutman, J. 1978, *Proc. IEEE*, **66**, 1048.
Seward, F. 1985, *Comments Ap.*, **11**, 15.
Shapiro, S. L., and Teukolsky, S. A. 1983, *Black Holes, White Dwarfs, and Neutron Stars* (New York: Wiley).
Standish, E. M., Keesey, M. S. W., and Newhall, X. X. 1976, *Jet Propulsion Lab. Tech. Rep. 32–1603*.

J. M. CORDES: Astronomy Department, Space Sciences Building, Cornell University, Ithaca, NY   14853.

G. S. DOWNS: Room B285, MIT Lincoln Laboratory, P.O. Box 73, Lexington, MA   02173.

J. KRAUSE-POLSTORFF: Department of Physics 61, Naval Postgraduate School, Monterey, CA   93940